SURFACE LOADING AND RIGID INDENTATION OF AN ELASTIC LAYER WITH SURFACE ENERGY EFFECTS

by

Xujun Zhao

M. Eng., Tsinghua University, P. R. China, 2007

A THESIS SUBMITTED IN PARTIAL FULLFILLMENT OF

THE REQUIREMENTS FOR THE DEGREE OF

MASTER OF APPLIED SCIENCE

in

THE FACULTY OF GRADUATE STUDIES

(MECHANICAL ENGINEERING)

THE UNIVERSITY OF BRITISH COLUMBIA

(Vancouver)

August 2009

Abstract

With the growing interest in nanotechnology, it is becoming important to understand the nanoscale mechanics to achieve successful design and fabrication of nanoscale devices. However, the classical continuum theory is not directly applicable to the analysis of nanoscale domains due to size-dependent behavior of nanostructures. Since the surface-to-volume ratio of a nanoscale domain is relatively high compared to that of a macro-scale domain, the energy associated with atoms at or near a free surface is different from that of atoms in the bulk. The effect of surface free energy therefore needs to be considered. Ultra-thin film/substrate systems, which are encountered in applications involving nanocoatings, nanotribology and material characterization based on nano-indentation, may be analyzed using modified continuum elasticity theory incorporating surface energy effects.

This thesis presents a set of analytical solutions for elastic field of a layer of nanoscale thickness bonded to a rigid base under surface loading and indentation by a rigid body. Surface energy effects are accounted for by using Gurtin-Murdoch elasticity theory. Fourier and Hankel integral transforms are used to solve the two- and three-dimensional boundary-value problems involving non-classical boundary conditions associated with the generalized Young-Laplace equation. In the case of a two-dimensional semi-infinite medium, the solutions can be expressed in closed form. The elastic field is found to depend on the layer thickness and surface elastic constants, and the influence of surface energy is shown to be more significant under a horizontal load than under a vertical load. A characteristic length scale related to the surface material properties can be identified for the present class of problems. The solution for the indentation problem is considered for flat, conical and spherical rigid indenters. The mixed boundary-value problem corresponding to a rigid indenter is formulated in terms of a dual integral equation system that is solved by using numerical quadrature. Selected numerical results are presented to show the influence of the indenter shape, surface properties and size-dependency of response.

Table of Contents

List of Figures

List of Symbols

a	Radius of loading area
d	Indentation depth
h	Thickness of elastic layers
$J_n(x)$	N-th order Bessel Functions of the first kind
$k_{\alpha\beta}$	Curvature tensor of surface
n_i	Unit normal vector in the *i*-direction
R	Radius of spherical indenter
$S_{\alpha\beta\gamma\delta}$	Surface elastic constant tensor
u_i	Displacement component in the *i*-direction
τ^s	Residual surface stress under unstrained condition
ε_{ij}	Strain component
σ_{ij}	Stress component
κ^s	Surface elastic modulus
λ , μ	Bulk lamé constants
λ^s , μ^s	Surface Lamé constants
Λ	Material characteristic length

Acknowledgements

I wish to express my greatest appreciation and gratitude to my supervisor, Dr. Nimal Rajapakse, for his guidance of this work and continuous support which enabled me to complete the thesis. I also gratefully acknowledge the support from Professor Nimal Rajapakse's research grant from the Natural Sciences and Engineering Research Council of Canada. I would also like to express my sincere thanks to Dr. Phani and Dr. Stoeber who serve as the members of my thesis committee and spend time and energy reading my thesis.

Finally, I want to thank my parents and my friends for their constant support, encouragement and help.

Chapter 1

INTRODUCTION

1.1 Nanotechnology

Nanoscience and nanotechnology is a relatively new research field which is primarily concerned with the discovery and exploration of the properties of materials whose constituent structures exist at the nanometer scale. The jargon 'nano' means a billionth, and a nanometer (nm) is 10^{-9} m (that is, the size of several atoms), which is roughly 10,000 times smaller than the diameter of a human hair. In the context of mechanical properties, 'nanometer scale' tends to mean less than 100 nm, whereas for electronic properties it means less than 10 nm [1].

Generally, scientific historians do not point to the beginning of nanoscience and nanotechnology until 1959, the year that Nobel Laureate physicist Richard Feynman gave his landmark speech to the American Physical Society entitled "There's Plenty of Room at the Bottom" [2], which is considered to lay the foundation to conceptualize and develop the research base for nanoscience and nanotechnology. He predicted that there would be some exciting new phenomena that might revolutionize science and technology and affect our daily life, if materials and structures were manipulated and assembled at the atomic level. Based on Feynman's idea, Drexler [3] advanced the idea of "molecular nanotechnology" in 1986 in the book *Engines of Creation*, where he postulated the concept of using a large number of robotic-like machines to form the basis of a molecular manufacturing technology that may build any structure directly using atoms and molecules. Since then, nanoscience and nanotechnology have grown quickly with the help, in large part, of the invention of the scanning tunneling microscope (STM) and atomic force microscope (AFM). As a result, many nanomaterials and nanostructures are developed, such as nanoparticles, nanotubes, nanowires, nanocomposites and nanofilms, which are widely used in many areas of application such as advanced materials, chemical sensors, biosensor, solar cells, drug delivery and nano-electromechanical systems (NEMS), etc. [4].

When the physical dimensions of materials and structures enter the nanoscale, the corresponding mechanical, electrical, optical, thermodynamic, and other types of properties are strongly modified and some fascinating behavior can be observed. Take the mechanical properties as an example, the carbon nanotube, first discovered by Iijima [5, 6], shows excellent mechanical properties with Young's modulus values of ~1TPa from the direct experimental measurements and atomistic simulations [7]. An ultra-thin membrane that is barely visible to the naked eye is reported to have supported a liquid body 70,000 times heavier than its own weight and withstand significant deformations [8]. When an isolated silicon nanoparticle is compressed using a diamond tip in Transmission Electron Microscopy (TEM), the results show that the compressible failure strain can be as high as 13%, which is much higher than brittle bulk silicon [9]. Ouyang et al [93] reported that nanoporous structures have a higher effective elastic modulus when the pore size approaches the nanoscale. Other experimental results show that both yield strength and fatigue lifetime of ultra-thin copper films are dependent on film thickness, and they increase with decreasing film thickness [10]. Nanostructured surface coatings can effectively improve the friction and wear-resistant properties of substrates in tribology. It is shown that the friction coefficient of a nanostructure coated material is lower than that of a conventional coated surface [11]. Moreover, nanoholes in a thin metal behave particularly remarkable manner and they can cause surface plasmons to couple and behave as if they are molecules. They absorb and reemit at least some light without converting it to a different form of energy [12]. In addition, nanoscience and nanotechnology have already found their way into the environment applications and geochemistry, and a further discussion can be found in Ref. [13]. Therefore, it is quite apparent that nanoscale materials and structures are used today pervasively and they cover a wide range of applications in science and technology.

1.2 Nanomechanics

In order to successfully design and develop nanoscale devices and systems, it is important to understand all fundamental aspects of the mechanical behavior of nanoscale materials and structures. There is therefore growing interest in the study of the mechanics

of nanoscale structures and devices. Nanomechanics, one of the founding pillars of nanoscience and nanotechnology, is a research field that considers the mechanical behavior and response at the nanoscale level. It plays an important role in comprehensive understanding of the mechanisms of deformation, stress field, strength and fracture of nanoscale materials and structures, which can be substantially different from the bulk materials.

In general, there are two basic approaches for the investigation of nanomechanics: theoretical simulations and experimental methods. The theoretical simulation methods include the broad areas of 'ab initio' quantum mechanics, the molecular dynamics (MD) and multi-scale methods. The atomistic modeling techniques dealing with the motion of atoms and simulating the behavior of objects in nanoscale domains based on the first-principle methods or semi-empirical interatomic potentials cannot be used to analyze large systems due to limitations in terms of the time and length scales. Although the classical MD simulations have become prominent as a tool for elucidating the complex physical phenomena at the nanoscale, the length and time scales that can be probed using MD simulations are still fairly limited. Based on coupling of atomistic and continuum models, some multiscale computational approaches are developed to simulate hierarchical structures [14, 15], in which the quantum calculation and the MD simulations are only used in localized regions where the atomic scale dynamics may be important, and the continuum simulation methods elsewhere. To some extent, these computational models are also currently limited in applications owing to the requirement of heavy computing resources. A comprehensive literature review on the computational nanomechanics and materials can be found in Ref. [16].

Nanomechanics studies require not only atomic and molecular modeling, but also modeling at both the mesoscopic and continuum scales, which is especially true for mechanical properties that depend on phenomena at all possible length scales [17]. Therefore, the application of continuum-based theoretical approaches is considered attractive due to their lesser complexity and computational efficiency. If we define the atomic models as a bottom-up approach from first-principles or classical MD, the

continuum-based models can be considered a top-down approach through building a refined continuum model to describe the nanoscale effects [18]. However, the classical concepts of continuum mechanics need to be modified to account for the quantum/molecular effects that exist at the nanoscale. Unlike the atomistic simulations that directly calculate the behavior atom by atom, the main idea behind the majority of the modified continuum models is to incorporate the interatomic potentials or atomistic properties into the continuum framework as some special parameters to account for the nanoscale effects. The surface energy effect, also called surface stress effect, is one of such significant effects that may greatly affect the mechanical properties and response of nanoscale materials and structures. The surface/interface energy effect acts only on the atom layers near or on the surface/interface, thus it cannot be felt in the bulk. However, it can no longer be neglected in nanostructured materials whose ratio of surface to volume is comparatively high. Such examples include nanobeams, nanoplates, nanoinhomogeneities and nanofilms. For example, Dingreville and Qu [19, 20] developed a continuum framework to incorporate the excess interfacial free energy into the conventional theory of continuum mechanics, and demonstrated that the overall elastic behavior of nanoscale structural elements is size-dependent.

The experimental nanomechanics refers to the quantitative experimental study of the mechanical behavior and response at the nanoscale level with the help of modern scientific testing equipments. Among the various techniques, scanning probe microscopy, e.g. STM and AFM, is an effective tool to investigate the individual nanostructures. Wong et al. [21] measured the mechanical properties of individual, structurally isolated silicon carbide nanorods and multi-wall carbon nanotubes (MWCNTs) directly using AFM. Yu et al. [22] and Peng et al. [7] developed AFM cantilever probe-based loading techniques and an in situ TEM method using a MEMS material testing system, respectively, with which tensile-loading experiments were carried out to determine the axial Young's modulus of MWCNTs and observe the failure patterns as well. Nano-indentation is another popular tool at present time to extract mechanical properties of materials at nanoscale, such as elastic modulus and hardness. In such tests an indenter of known geometry is pressed into the surface and the relation of load and indenter

displacement is continuously recorded to determine the mechanical properties of surface coatings and thin films [23-25]. These instruments allow precise control of either the load or displacement during the test and can be used to apply forces as low as a few micro-newtons to make indentation depths in the nanometer range [26]. Oliver and Pharr [27] established an improved method for determining the hardness and elastic modulus from nano-indentation load-displacement data by examining six materials. Mao et al. [28] and Li et al. [29] investigated the mechanical properties of semiconducting ZnO nanobelts and silver nanowires by using nano-indentation, respectively. Their results show that the nano-indentation technique is a promising tool for material testing. However, more advances in experimental methods are needed that could provide direct information on the material properties at all length scales of interest to validate the results from theoretical and numerical modeling.

1.3 Review of Surface Elasticity Model

The seminal concepts of surface energy and surface stress were originally formulated by Gibbs [30], who defined a quantity γ, known as excess surface free energy, to represent the reversible work per unit area owing to creating a new surface by a process such as cleavage or creep. Gibbs also pointed out that there is another surface quantity for solids that is associated with the reversible work per unit area needed to elastically stretch a pre-existing surface. Since then the surface energy effect has attracted substantial attention and Gibbsean thermodynamics has been extended for better understanding of many aspects of surface physics [31-35]. It has been recognized that the surface thermodynamics is one of the most useful and powerful tools for studying various surface phenomena, such as surface reconstruction, self-assembled domain patterns, phase transformation, epitaxial growth and so on.

From the thermodynamics of solid surfaces, the relationship between the surface stress and surface free energy has been formulated as [32, 36]

$$\sigma_{\alpha\beta} = \gamma\delta_{\alpha\beta} + \partial\gamma/\partial\varepsilon_{\alpha\beta} \tag{1.1}$$

where $\sigma_{\alpha\beta}$ and $\varepsilon_{\alpha\beta}$ denote the surface stress and strain, respectively, and $\delta_{\alpha\beta}$ is the Kronecker delta.

In contrast to the excess surface free energy γ, which is a scalar, the surface stress is a second rank tensor in the tangent plane of the surface and the strain normal to the surface is excluded in Eq. (1.1). Thus, the Greek indices take the value of 1 or 2. Clearly, the surface stress is composed of the surface free energy part that is strain-independent, and its derivative with respect to strain. It should be noted that the second term in the right-hand side vanishes for a liquid due to the fact that atoms from the bulk are free to migrate to the surface when a liquid surface deforms so that the atom density at the surface remains roughly a constant in the process of deformation. However, for solids, it is not the case and the surface stress therefore is stain-dependent. Nix and Gao [37] presented a clear atomistic interpretation of the interface stress and showed that Eq. (1.1) is an expression in the Eulerian frame of reference and the first term does not appear in the embedded Lagrangian coordinates.

The excess surface energy γ can be understood as a superficial energy term since a surface can be interpreted as a layer to which a certain energy is attached [34]. Due to the different local environment, atoms at or near a free surface or interface have different equilibrium positions than do atoms in the bulk of a material. As a result, the energy of these atoms is, in general, different from that of the atoms in the bulk [19]. It can also be interpreted that the reduced coordination of atoms near or in the surface layer vs. atoms within the bulk induces a corresponding redistribution of electronic charge, and the altered binding situation in the surface is the modified layer spacing, which deviates in general from the bulk values [38]. Thus, the energy associated with atoms near or at the surface may differ from those in the bulk. The ratio of surface free energy $\gamma\,(J/m^2)$ and Young's modulus $E\,(J/m^3)$, γ/E, is dimensional (m) and points to some other inherent parameter of a material. This intrinsic length scale is usually small, in the nanometer range or even smaller. When a material element has one characteristic length comparable to the intrinsic scale, the surface/interface free energy can play an important role in its properties and behavior. The effect of surface free energy therefore becomes important in nanoscale problems and leads to some size-dependent behavior. In addition, for some soft solids, such as polymer gels and biological materials, the surface energy (hence surface

stresses) may also have an important influence on surface topographical patterns. Consequently, the study of the elastic field of a solid with surface energy effects is of interest to many current technological developments.

Surface energy effects are generally ignored in traditional continuum mechanics. However, this is not the case for nanoscale structures due to their high surface/volume ratio, soft materials where the ratio of surface energy per unit area to the bulk Young's modulus is comparable to the characteristic size of a material element and other situations where the surface tension gradient and other surface energy driven effects have a significant influence on the response. By analogy to the linear constitutive equations of bulk materials, Miller and Shenoy [39] introduced a set of surface elastic constants and suggested a linear surface constitutive relation of the following form:

$$\sigma_{\alpha\beta} = \tau^0 \delta_{\alpha\beta} + S_{\alpha\beta\gamma\delta}\varepsilon_{\varphi\delta} \tag{1.2}$$

where $\tau^0_{\alpha\beta}$ is the surface residual stress under unstrained conditions, and $S_{\alpha\beta\gamma\delta}$ is the fourth order surface elastic stiffness tensor.

Based on a rigorous mathematical formulation, Gurtin and Murdoch [40-42] developed a theoretical framework based on the continuum mechanics concepts that included the effects of surface and interfacial energy, in which the surface is modeled as a mathematical layer of zero thickness perfectly bonded to an underlying bulk. The surface (interface) has its own properties and processes that are different from the bulk. For an isotropic elastic surface, the generic expression for surface stress-strain relation has the following form.

$$\sigma^s_{\beta\alpha} = \tau^s \delta_{\beta\alpha} + 2\left(\mu^s - \tau^s\right)\varepsilon_{\beta\alpha} + \left(\lambda^s + \tau^s\right)\varepsilon_{\gamma\gamma}\delta_{\beta\alpha} + \tau^s u^s_{\beta,\alpha} \tag{1.3}$$

where the superscript '*s*' is used to denote the quantities corresponding to the surface; μ^s and λ^s are surface Lamé constants; τ^s is the residual surface tension under unstrained conditions, which is a constant.

It should be pointed out that the surface elastic constants have dimensions of Newton per meter (N/m), which is different from the bulk elastic constants, because the surface stress exists on a two-dimensional surface. With the assumption of isotropy, Miller and Shenoy [39] computed the values of the surface moduli for different surface orientations using the embedded atom method (EAM) and Stillinger-Weber empirical potentials. Dingreville and Qu [43, 44] presented a semi-analytical method to compute the surface elastic constants of several FCC metals. A systematic study of the surface elastic constants has been performed by Shenoy [45] and their values can be calculated from atomistic simulations. Recently, Mi et al. [46] performed an atomistic calculation of interface elastic properties in noncoherent metallic bilayers. From their results, it is found that the surface elastic constants are dependent on crystalline orientation. Moreover, they need not be positive definite. Therefore, the quadratic form $S_{\alpha\beta\gamma\delta}\varepsilon_{\alpha\beta}\varepsilon_{\gamma\delta}$ may be negative, but it does not violate the basic thermodynamic postulates, because a surface region with a special atomic structure cannot exist without the bulk and the total energy (bulk + surface) still satisfies the positive definite condition [45]. It is noted that the assumption of zero-thickness surface/interface is just an idealization of a complex problem. If the number of atoms in the bulk is comparable to that of the surface layer, the surface/interface model is not applicable in this case.

Although the experimental measurement of surface elastic constants seems to be a challenging task, some attempts have already been made. Jing et al. [47] determined the surface elastic properties of silver nanowires by using three-point bending test and contact atomic force microscopy. They found that surface elastic modulus E^s and surface residual stress τ^s are 8.7 N/m and 5.8 N/m, respectively, which are of the same order as the values determined from atomistic simulations.

The surface elasticity model is extensively used in the nanomechanics to explain the size-dependent behavior at the nanoscale. Miller and Shenoy [39] demonstrated that size-dependent behavior of nanoscale structural elements can be modeled by applying the Gurtin-Murdoch continuum model with surface stress, whose results are almost indistinguishable from the atomistic simulations for nanoplates. He and Lilley [48, 49]

examined the elastic responses of static and dynamic bending of nanowires under different boundary conditions by considering the surface effect. Wang and Feng [50] studied the similar problems and discussed the effects of surface elasticity and residual surface tension on the natural frequency of microbeams. Their results show that both the surface elastic modulus and residual surface tension contribute to the elastic deformation and natural frequency of microbeams and nanowires. In contrast, Gurtin et al. [51] showed that the beam resonant frequency is independent of the residual surface stress within the framework of linear elastic beam theory, and this finding has also been validated by subsequent researchers, for example by Lu et al. [52] and Lachut and Sader [53]. Recent work by Park [54] has shown that the influence of the residual surface stress on the resonant frequencies of silicon nanowires takes places only if finite deformation kinematics is considered. The surface effects on the thin plate theory were also examined by applying Gurtin-Murdoch continuum model [55-57].

The continuum theory of surface elasticity was further developed by many researchers to analyze the problems of nano-inhomogeneities. For example, Sharma and co-workers [58, 59] analyzed the size-dependent elastic field of spherical and ellipsoidal nano-inclusions by applying Gurtin-Murdoch model with both residual surface stress and strain-dependent surface stresses. Tian and Rajapakse [60, 61] examined the size-dependent elastic field due to nano-scale circular and elliptical defects in an isotropic matrix respectively and observed unstable defect geometries. Based on a micromechanics framework, Duan et al. [62-64] extended the Eshelby' formalism for nanoscale spherical inhomogeneities subjected to arbitrary uniform eigenstrain by considering surface/interface effects, and demonstrated that the effective moduli of composites containing spherical nano-particles are size-dependent and the Eshelby tensors and stress concentration tensors are, in general, not uniform inside the inhomogeneity but are size- and position-dependent. A more recent review article provides further information on this topic [65]. Gao et al. [66] and Tian and Rajapakse [67] independently developed finite element methods (FEM) by introducing the surface elements to take into account the surface energy effects and then applied the method to investigate elastic inhomogeneity problems with complex geometry and loading.

1.4 Review of Contact Mechanics of Films/substrates

Thin film/substrate systems permeate many engineering applications such as microelectronics, integrated circuits, magnetic information storage systems, optical filters, wear and corrosion resistant coatings, etc. According to William Nix [68], although we typically think of thin film based devices in terms of their electronic, magnetic or optical properties, many such devices are limited by their mechanical properties. Consequently, it is of great importance to understand the mechanical performance and reliability of film/substrate systems. Vinci and Vlassak [69] reviewed the mechanical behavior of thin films, and introduced the main experimental techniques for the measurement of thin film properties. Mishnaevshy Jr. and Cross [70] reviewed the theoretical models and methods of analysis of deformation, damage and fracture based on classical continuum mechanics for thin film/substrate systems. The related problems of plastic deformation, cracks, as well as the effects of dislocation were also discussed by them. Recently, Feng et al. [71] and Ngo et al. [72] studied the stress field in a multilayer thin film/substrate system subjected to non-uniform temperature and misfit strains based on an extension of the classical Stoney formula.

An interesting class of problems in thin film/substrate systems deals with the contact mechanics of a surface-loaded layer bonded to an underlying base, which has a wide range of practical applications in the mechanics of microelectronics devices, nano-indentation, and surface coatings. Poulos [73] solved the plane problem for a vertically loaded strip and presented the stresses and displacements in an elastic layer underlain by a rough rigid base. Harding and Sneddon [74] and Sneddon [75] obtained the analytical solutions for a rigid punch with an arbitrary profile in a semi-infinite solid by using Hankel integral transform techniques. The flat-ended rigid cylindrical indenter problem for an elastic layer resting frictionlessly on a rigid base was solved by Lebedev and Ufliand [76]. Dhaliwal and Rau [77, 78] reduced the axisymmetric Boussinesq problem of an elastic layer lying over an elastic half-space to a Fredholm integral equation that was solved numerically to obtain the elastic field. Yu et al. [79] examined the effect of a substrate on the elastic properties of films by using indentation tests and several

combinations of film and substrate elastic moduli and film thicknesses were considered. Recently, inspired by multidimensional nano-contact mechanics experiments for the measurement of both the normal and tangential contact stiffness of film/substrate systems [80], Gao et al. [81] gave an analytical formulation to predict the effective elastic modulus of film-on-substrate systems under normal and tangential contact.

Nowadays, a film can be fabricated as thin as few nanometers by taking advantage of modern processing technologies. Due to the high ratio of surface to volume of nanofilms, it is necessary to consider the surface energy effect, which is usually neglected in classical mechanics. The Gurtin-Murdoch surface stress model has recently been employed to study the modern contact problems. Povstenko [82] derived the elastic field of a half-space caused by a jump in the surface tension over a circular area by neglecting the bulk properties. He and Lim [83] derived the surface Green's functions of a soft *incompressible* isotropic elastic half-space with surface energy effects by using the Gurtin-Murdoch model. In addition to the incompressibility, they further restricted their derivation to the special case where the surface elastic properties are same as the bulk properties. Wang and Feng [84] studied the response of a half-plane subjected to surface pressures by neglecting the surface elastic constants and considering only the influence of constant surface tension. Their results show that both the contact normal stress and the deformations depend strongly on the surface residual stress, which are obviously different from that obtained by Povstenko [82] and the results of Huang and Yu [85], who considered a surface-loaded half-plane with non-zero surface elastic constants. Based on the surface elasticity theory, Koguchi [86] presented Green's functions for an anisotropic elastic half-space using Stroh's formalism.

1.5 Objective and Scope of the Current Work

Based on the above introduction and literature survey, it can be seen that further development of the solutions based on the Gurtin-Murdoch theory of elasticity accounting for the surface energy effects is important to the study of the mechanics of nanoindentation, nanofilms and nanocoatings. In addition, this class of problems dealing with a continuum with surface energy effects also has applications in the study of very

soft materials such as biological materials and polymer gels and their surface effects. The past studies have concentrated on the simple problems of a semi-infinite medium loaded at the surface whereas the focus of this thesis is on the more practical case of an elastic layer on a rigid substrate. In addition, no past study has examined the classical indentation problems involving a rigid punch in the presence of surface energy effects even in the special case of a semi-infinite medium. The objective of this thesis is therefore to examine the behavior of a thin-layer of elastic material bonded to a rigid substrate by using the Gurtin-Murdoch continuum theory. Problems related to vertical and tangential loading and rigid indenters are considered to understand the importance of nanoscale effects in thin layers and the applicability of modified continuum approaches for modeling of nanoindentation.

Chapter 2 presents a detailed derivation of an analytical solution for a compressible isotropic elastic layer that is perfectly bonded to a rigid base and subjected to surface loading. Complete surface stress effects (non-zero surface tension and surface elastic properties) are considered in the derivation. Both two-dimensional plane and axisymmetric problems are considered. The Fourier and Hankel integral transforms are used to solve the boundary-value problems involving non-classical boundary conditions associated with the generalized Young-Laplace equation. Closed-form analytical solutions are presented for the case of a layer of infinite thickness (half-plane/space) and in this case the influence of surface energy effects can be explicitly identified. For a layer of finite thickness, the elastic field is examined numerically to assess the influence of surface energy effects and layer thickness.

Chapter 3 considers the general three-dimensional asymmetric problems for an elastic layer that is bonded to a rigid substrate and subjected to tangential loading at the surface. Muki's method [87] is extended to investigate the elastic field based on the Gurtin-Murdoch model. The Hankel integral transforms are used to solve the non-classical boundary value problems related to a tangential concentrated load and a uniformly distributed circular patch load in the tangential direction. The analytical solutions are obtained for the corresponding boundary-value problems. Selected

numerical results are presented to illustrate the influence of surface energy effects on tribology and the tangential stiffness of nano-coatings and ultra-thin films.

In chapter 4, the contact problems for an elastic half space indented by indenters with different profiles are investigated by applying the surface elasticity model. The medium is assumed isotropic and the indenter is rigid. The analytical solution of the corresponding axisymmetric mixed boundary value problem is formulated by using the Hankel integral transforms, and the resulting Fredholm Integral Equation of the second kind is solved numerically. The influence of the surface stress effect on the elastic field and vertical stiffness is presented for different indenter profiles, contact areas and material properties.

Finally, chapter 5 presents a summary of the thesis, major findings of the current study and suggestions for future work.

Chapter 2

PLANE AND AXISYMMETRIC ELASTIC FIELDS OF A SURFACE-LOADED THIN LAYER IN THE PRESENCE OF SURFACE STRESSES

2.1 Problem Description and Basic Equations

In this chapter, both two-dimensional plane and axisymmetric problems for an isotropic elastic thin film on a rigid substrate are considered in the presence of surface stresses. Consider an elastic layer of finite thickness bonded to a rigid base as shown in Fig. 2.1 and subjected to surface loading. According to the Gurtin-Murdoch model, the surface energy effects are accounted for by considering the surface as a mathematical layer of zero thickness with relevant elastic properties and residual surface tension. The governing equations of the bulk material are the same as those in the classical elasticity. In addition, on a surface (or interface), the generalized Young-Laplace equation [40, 82] and a set of constitutive relations have to be satisfied. The basic equations for small displacements and infinitesimal strains of a continuum with surface stress effects are summarized below based on Gurtin et al.[40, 42].

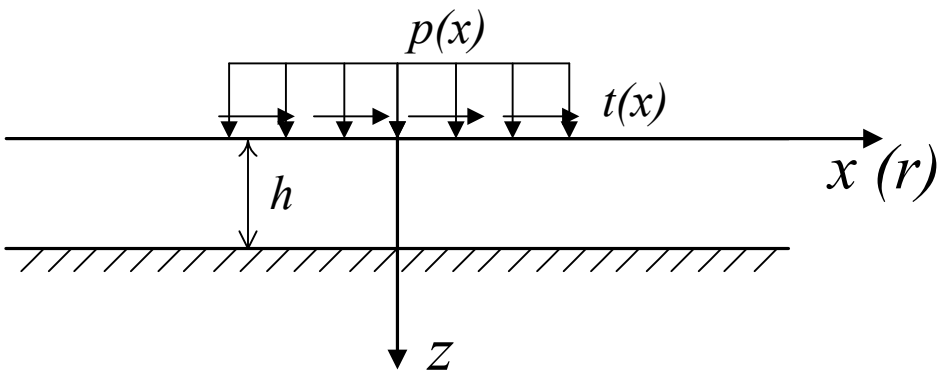

Fig. 2.1 Elastic layer subjected to surface loading.

In the absence of body forces, the three-dimensional equilibrium and constitutive equations of the bulk material are,

$$\sigma_{ij,j} = 0 \tag{2.1}$$

$$\sigma_{ij} = 2\mu\varepsilon_{ij} + \lambda\delta_{ij}\varepsilon_{kk} \tag{2.2}$$

and the classical strain-displacement relationship is,

$$\varepsilon_{ij} = \frac{1}{2}\left(u_{i,j} + u_{j,i}\right) \tag{2.3}$$

where u_i , σ_{ij} and ε_{ij} denote the components of displacement, stress and strain tensors respectively; and μ and λ are Lamé constants of the bulk material.

On the surface, the generalized Young-Laplace equation [82], surface constitutive relations and strain-displacement relationship can be expressed as [40, 41]

$$\sigma^s_{\beta\alpha,\beta} + \sigma_{j\alpha} n_j = 0\,, \quad \sigma_{ji} n_i n_j = \sigma^s_{\beta\alpha} k_{\beta\alpha} \tag{2.4}$$

$$\sigma^s_{\beta\alpha} = \tau^s \delta_{\beta\alpha} + 2\left(\mu^s - \tau^s\right)\varepsilon_{\beta\alpha} + \left(\lambda^s + \tau^s\right)\varepsilon_{\gamma\gamma}\delta_{\beta\alpha} + \tau^s u^s_{\beta,\alpha} \tag{2.5}$$

$$\varepsilon^s_{\alpha\beta} = \frac{1}{2}\left(u^s_{\alpha,\beta} + u^s_{\beta,\alpha}\right) \tag{2.6}$$

where the superscript '*s*' is used to denote the quantities corresponding to the surface; μ^s and λ^s are surface Lamé constants; τ^s is the residual surface tension under unstrained conditions; n_i denotes the components of the unit normal vector of the surface; and $k_{\beta\alpha}$ is the curvature tensor of the surface.

It should be noted that the surface stress tensor is a 2D quantity and the strain normal to the surface is excluded in Eq. (2.5). Thus, the Greek indices take the value of 1 or 2, while Latin subscripts adopt values from 1 to 3.

Shenoy [45] and Cammarata [32] have reported the values of the surface stress at zero strain (τ^s) for different surface orientations of pure metals and semiconductors by using first-principles calculations or atomistic potential methods. There are also experimental measurements cited by Cammarata [32]. By definition these values are

constant for a given surface orientation of a pure metal/semiconductor at a specific temperature. Presence of impurities and vacancies have an influence on the value of τ^s.

2.2 General Solutions of Bulk Material

The general solution for displacements and stresses of a two-dimensional elastic solid can be expressed with respect to a Cartesian coordinate system (Fig.1) by using Fourier integral transforms as [88, 89],

$$
\begin{aligned}
u_z &= \frac{1}{4\pi\mu}\int_{-\infty}^{+\infty}\left\{\left[A|\xi|+\left(\frac{\mu}{\mu+\lambda}+z|\xi|\right)B\right]e^{-|\xi|z}+\left[-C|\xi|+\left(\frac{\mu}{\mu+\lambda}-z|\xi|\right)D\right]e^{|\xi|z}\right\}e^{-i\xi x}d\xi \\
u_x &= \frac{1}{4\pi\mu}\int_{-\infty}^{+\infty}\left\{\left[A\xi-\left(\frac{\lambda+2\mu}{\mu+\lambda}\frac{|\xi|}{\xi}-z|\xi|\right)B\right]e^{-|\xi|z}\right. \\
&\qquad \left.+\left[C\xi+\left(\frac{\lambda+2\mu}{\mu+\lambda}\frac{|\xi|}{\xi}+z|\xi|\right)D\right]e^{|\xi|z}\right\}ie^{-i\xi x}d\xi
\end{aligned}
\tag{2.7}
$$

$$
\begin{aligned}
\sigma_{zz} &= -\frac{1}{2\pi}\int_{-\infty}^{+\infty}\xi^2\left[(A+Bz)e^{-|\xi|z}+(C+Dz)e^{|\xi|z}\right]e^{-i\xi x}d\xi \\
\sigma_{xx} &= \frac{1}{2\pi}\int_{-\infty}^{+\infty}\left\{\left[A\xi^2-\left(2|\xi|-z\xi^2\right)B\right]e^{-|\xi|z}+\left[C\xi^2+\left(2|\xi|+z\xi^2\right)D\right]e^{|\xi|z}\right\}e^{-i\xi x}d\xi \\
\sigma_{xz} &= \frac{1}{2\pi}\int_{-\infty}^{+\infty}i\xi\left\{\left[A|\xi|+\left(1-z|\xi|\right)B\right]e^{-|\xi|z}+\left[C|\xi|+\left(1+z|\xi|\right)D\right]e^{|\xi|z}\right\}e^{-i\xi x}d\xi
\end{aligned}
\tag{2.8}
$$

where $A(\xi)$, $B(\xi)$, $C(\xi)$ and $D(\xi)$ are arbitrary functions to be determined from the boundary conditions.

In the case of axisymmetric problems, the general solutions for displacements and stresses can be expressed in terms of a cylindrical coordinate system (r, θ, z) by using Hankel integral transforms as [88, 89],

$$
\begin{aligned}
u_r &= \frac{\lambda+\mu}{\mu}\int_0^\infty \xi^2 \left\{\left[-A'\xi+(1-z\xi)B'\right]e^{-\xi z}+\left[C'\xi+(1+z\xi)D'\right]e^{\xi z}\right\}J_1(\xi r)\,d\xi \\
u_z &= -\frac{\lambda+\mu}{\mu}\int_0^\infty \xi^2 \left\{\left[A'\xi+\left(\frac{2\mu}{\lambda+\mu}+z\xi\right)B'\right]e^{-\xi z}+\left[C'\xi-\left(\frac{2\mu}{\lambda+\mu}-z\xi\right)D'\right]e^{\xi z}\right\}J_0(\xi r)\,d\xi
\end{aligned}
\tag{2.9}
$$

$$
\begin{aligned}
\frac{\sigma_{rr}}{2(\lambda+\mu)} &= \int_0^\infty \xi^3 \left\{\left[-A'\xi+\left(\frac{2\lambda+\mu}{\mu+\lambda}-z\xi\right)B'\right]e^{-\xi z}+\left[C'\xi+\left(\frac{2\lambda+\mu}{\mu+\lambda}+z\xi\right)D'\right]e^{\xi z}\right\}J_0(\xi r)\,d\xi \\
&\quad -\frac{1}{r}\int_0^\infty \xi^2 \left\{\left[-A'\xi+(1-z\xi)B'\right]e^{-\xi z}+\left[C'\xi+(1+z\xi)D'\right]e^{\xi z}\right\}J_1(\xi r)\,d\xi \\
\frac{\sigma_{\theta\theta}}{2(\lambda+\mu)} &= \frac{\lambda}{\mu+\lambda}\int_0^\infty \xi^3 \left(B'e^{-\xi z}+D'e^{\xi z}\right)J_0(\xi r)\,d\xi \\
&\quad +\frac{1}{r}\int_0^\infty \xi^2 \left\{\left[-A'\xi+(1-z\xi)B'\right]e^{-\xi z}+\left[C'\xi+(1+z\xi)D'\right]e^{\xi z}\right\}J_1(\xi r)\,d\xi \\
\frac{\sigma_{zz}}{2(\lambda+\mu)} &= \int_0^\infty \xi^3 \left\{\left[A'\xi+\left(\frac{\mu}{\mu+\lambda}+z\xi\right)B'\right]e^{-\xi z}+\left[-C'\xi+\left(\frac{\mu}{\mu+\lambda}-z\xi\right)D'\right]e^{\xi z}\right\}J_0(\xi r)\,d\xi \\
\frac{\sigma_{rz}}{2(\lambda+\mu)} &= \int_0^\infty \xi^3 \left\{\left[A'\xi-\left(\frac{\lambda}{\mu+\lambda}-z\xi\right)B'\right]e^{-\xi z}+\left[C'\xi+\left(\frac{\lambda}{\mu+\lambda}+z\xi\right)D'\right]e^{\xi z}\right\}J_1(\xi r)\,d\xi
\end{aligned}
\tag{2.10}
$$

where $J_n(\xi)$ denotes the *n*-th order Bessel Functions of the first kind, and the arbitrary functions A', B', C' and D' are to be determined from the boundary conditions.

In the case of two-dimensional plane problems, the boundary conditions for the problem shown in Fig. 2.1 can be expressed as,

$$\sigma_{zz}\big|_{z=0} = -p(x) \tag{2.11}$$

$$\sigma_{xz}\big|_{z=0} + t(x) = -\left(\frac{d\tau^s}{dx} + \kappa^s \left.\frac{d^2 u_x}{dx^2}\right|_{z=0}\right) \tag{2.12}$$

$$u_z\big|_{z=h} = 0 \tag{2.13}$$

$$u_x\big|_{z=h} = 0 \tag{2.14}$$

where *p(x)* and *t(x)* denote the magnitude of applied surface loading in the *z*- and *x*-directions respectively; and $\kappa^s = 2\mu^s + \lambda^s$, is a surface material constant.

Application of Fourier integral transforms to eqns. (2.11) – (2.14) together with the assumption that surface tension is constant and the substitution of eqn. (2.7) results in,

$$A + C = \frac{\overline{p}(\xi)}{\xi^2} \tag{2.15}$$

$$B + D - (A - C)|\xi| + \frac{\bar{t}(\xi)}{i\xi} = \frac{\kappa^s}{2\mu}\left[\frac{\lambda + 2\mu}{\lambda + \mu}(D - B)|\xi| + (A + C)\xi^2\right] \tag{2.16}$$

$$\left[\frac{\mu}{\lambda + \mu}B + (A + Bh)|\xi|\right]e^{-|\xi|h} + \left[\frac{\mu}{\lambda + \mu}D - (C + Dh)|\xi|\right]e^{|\xi|h} = 0 \tag{2.17}$$

$$\left[-\frac{\lambda + 2\mu}{\lambda + \mu}B + (A + Bh)|\xi|\right]e^{-|\xi|h} + \left[\frac{\lambda + 2\mu}{\lambda + \mu}D + (C + Dh)|\xi|\right]e^{|\xi|h} = 0 \tag{2.18}$$

and

$$\begin{aligned} \overline{p}(\xi) &= \int_{-\infty}^{+\infty} p(x)e^{i\xi x}dx \\ \overline{t}(\xi) &= \int_{-\infty}^{+\infty} t(x)e^{i\xi x}dx \end{aligned} \tag{2.19}$$

Equations (2.15) – (2.18) can be solved to determine the coefficients A, B, C, and D appearing in Eq. (2.7) and (2.8). The following solutions are obtained.

$$\begin{aligned} A &= \frac{(A_p + iA_t)}{F}; \qquad B = \frac{(B_p + iB_t)}{F} \\ C &= \frac{(C_p + iC_t)}{F}; \qquad D = \frac{(D_p + iD_t)}{F} \end{aligned} \tag{2.20}$$

where

$$A_p = \frac{\overline{p}(\xi)}{2\xi^2}\left\{(\lambda + 3\mu)\left[(1 + \Lambda|\xi|)e^{2|\xi|h} - \Lambda|\xi|\right] + 2h\xi^2(\lambda + \mu)(\Lambda + h) - \frac{2(\lambda + \mu)^2}{\lambda + 2\mu}\Lambda h^2|\xi|^3 \right.$$
$$\left. -2(\lambda + \mu)h|\xi| + \frac{\lambda^2 + 4\lambda\mu + 5\mu^2}{\lambda + \mu}\right\}$$

$$B_p=\frac{\bar{p}(\xi)}{2|\xi|}\Bigg\{(\lambda+3\mu)\Bigg[\left(1+\frac{\lambda+\mu}{\lambda+2\mu}\Lambda|\xi|\right)e^{2|\xi|h}-\frac{\lambda+\mu}{\lambda+2\mu}\Lambda|\xi|\Bigg]$$
$$+\frac{2(\lambda+\mu)^2}{\lambda+2\mu}\Lambda h\xi^2+(\lambda+\mu)(1-2h|\xi|)\Bigg\}$$

$$C_p=\frac{\bar{p}(\xi)}{2\xi^2}\Bigg\{(\lambda+3\mu)\Big[(1-\Lambda|\xi|)e^{-2|\xi|h}+\Lambda|\xi|\Big]+\frac{2(\lambda+\mu)^2}{\lambda+2\mu}\Lambda h^2|\xi|^3$$
$$+2h\xi^2(\lambda+\mu)(\Lambda+h)+2(\lambda+\mu)h|\xi|+\frac{\lambda^2+4\lambda\mu+5\mu^2}{\lambda+\mu}\Bigg\} \tag{2.21}$$

$$D_p=-\frac{\bar{p}(\xi)}{2|\xi|}\Bigg\{(\lambda+3\mu)\Bigg[\left(1-\frac{\lambda+\mu}{\lambda+2\mu}\Lambda|\xi|\right)e^{-2|\xi|h}+\frac{\lambda+\mu}{\lambda+2\mu}\Lambda|\xi|\Bigg]$$
$$+\frac{2(\lambda+\mu)^2}{\lambda+2\mu}\Lambda h\xi^2+(\lambda+\mu)(1+2h|\xi|)\Bigg\}$$

.

$$A_t=-\frac{\bar{t}(\xi)}{|\xi|\xi}\left[\frac{\mu(\lambda+2\mu)}{\lambda+\mu}+(\lambda+\mu)h^2\xi^2\right]$$

$$B_t=\frac{\bar{t}(\xi)}{2\xi}\Big[(\lambda+3\mu)e^{2|\xi|h}+(\lambda+\mu)(1+2h|\xi|)\Big]$$

$$C_t=\frac{\bar{t}(\xi)}{|\xi|\xi}\left[\frac{\mu(\lambda+2\mu)}{\lambda+\mu}+(\lambda+\mu)h^2\xi^2\right]$$

$$D_t=\frac{\bar{t}(\xi)}{2\xi}\Big[(\lambda+3\mu)e^{-2|\xi|h}+(\lambda+\mu)(1-2h|\xi|)\Big]$$

$$F=(\lambda+3\mu)\big[\cosh(2\xi h)+\Lambda\xi\sinh(2\xi h)\big]+2h\xi^2(\lambda+\mu)(\Lambda+h)+\frac{\lambda^2+4\lambda\mu+5\mu^2}{\lambda+\mu}$$

and

$$\Lambda=\frac{\kappa^s(\lambda+2\mu)}{2\mu(\lambda+\mu)} \tag{2.22}$$

Note that Λ is a parameter with the dimension of length and represents a ratio of surface to bulk elastic properties. It can be viewed as a material characteristic length that represents the influence of surface energy effects. It is clear from the above solution that Λ solely quantifies the influence of surface elastic properties on the elastic field. Note

that Λ vanishes in the absence of surface stress effects and the above solution reduces to the classical elasticity solution.

The boundary conditions corresponding to axisymmetric vertical loading of the system shown in Fig. 1 can be expressed as,

$$\sigma_{zz}\big|_{z=0} = -p(r) \tag{2.23}$$

$$\sigma_{rz}\big|_{z=0} = -\left[\frac{d\tau^s}{dr}\left(1+\frac{u_r}{r}\right)_{z=0} + \kappa^s\left(\frac{d^2u_r}{dr^2}+\frac{1}{r}\frac{du_r}{dr}-\frac{u_r}{r}\right)_{z=0}\right] \tag{2.24}$$

$$u_r\big|_{z=h} = 0 \tag{2.25}$$

$$u_z\big|_{z=h} = 0 \tag{2.26}$$

Assuming that surface residual stress τ^s is constant along the radial direction and taking Hankel integral transforms of eqns. (2.23) – (2.26) together with the use of eqn. (2.9) leads to the following equations to determine the unknown arbitrary functions.

$$\mu(B'+D')+(\lambda+\mu)(A'-C') = \frac{Z(\xi)}{2\xi^2} \tag{2.27}$$

$$\lambda(D'-B')+(\lambda+\mu)(A'+C')\xi = \frac{\kappa^s\xi(\lambda+\mu)}{2\mu}\left[(B'+D')-(A'-C')\xi\right] \tag{2.28}$$

$$\left[B'-(A'+B'h)\xi\right]e^{-\xi h}+\left[D'+(C'+D'h)\xi\right]e^{\xi h} = 0 \tag{2.29}$$

$$\left[2B'+\frac{\lambda+\mu}{\mu}(A'+B'h)\xi\right]e^{-\xi h}-\left[2D'-\frac{\lambda+\mu}{\mu}(C'+D'h)\xi\right]e^{\xi h} = 0 \tag{2.30}$$

where

$$Z(\xi) = -\int_0^\infty rp(r)J_0(\xi r)dr \tag{2.31}$$

The solution of eqns. (2.27) – (2.30) yields the following solutions for the arbitrary functions *A'*, *B'*, *C'* and *D'*.

$$A' = \frac{1}{4}\frac{(A_0+A_1)}{F}\frac{Z(\xi)}{\xi^3}; \qquad B' = \frac{1}{4}\frac{(B_0+B_1)}{F}\frac{Z(\xi)}{\xi^2} \tag{2.32}$$

$$C' = \frac{1}{4}\frac{(C_0 + C_1)}{F}\frac{Z(\xi)}{\xi^3}; \qquad D' = \frac{1}{4}\frac{(D_0 + D_1)}{F}\frac{Z(\xi)}{\xi^2}$$

where

$$\begin{aligned}
A_0 &= \frac{\lambda(\lambda+3\mu)}{(\lambda+\mu)^2}e^{2\xi h} + 2h^2\xi^2 - \frac{2\lambda h\xi}{\lambda+\mu} + \frac{\lambda+3\mu}{\lambda+\mu} \\
A_1 &= \frac{\Lambda\xi}{\lambda+2\mu}\left[(\lambda+3\mu)\left(e^{2\xi h}-1\right) - 2h\xi(\lambda+\mu)(h\xi-1)\right] \\
B_0 &= \frac{\lambda+3\mu}{\lambda+\mu}e^{2\xi h} + (1-2h\xi) \\
B_1 &= \frac{\Lambda\xi}{\lambda+2\mu}\left[(\lambda+3\mu)\left(e^{2\xi h}-1\right) + 2h\xi(\lambda+\mu)\right] \\
C_0 &= -\left[\frac{\lambda(\lambda+3\mu)}{(\lambda+\mu)^2}e^{-2\xi h} + 2h^2\xi^2 + \frac{2\lambda h\xi}{\lambda+\mu} + \frac{\lambda^2+3\mu\lambda+4\mu^2}{(\lambda+\mu)^2}\right] \\
C_1 &= -\frac{\Lambda\xi}{\lambda+2\mu}\left[(\lambda+3\mu)\left(1-e^{-2\xi h}\right) + 2h\xi(\lambda+\mu)(h\xi+1)\right] \\
D_0 &= \frac{\lambda+3\mu}{\lambda+\mu}e^{-2\xi h} + (1+2h\xi) \\
D_1 &= \frac{\Lambda\xi}{\lambda+2\mu}\left[(\lambda+3\mu)\left(1-e^{-2\xi h}\right) + 2h\xi(\lambda+\mu)\right]
\end{aligned} \tag{2.33}$$

$$F = (\lambda+3\mu)\left[\cosh(2\xi h) + \Lambda\xi\sinh(2\xi h)\right] + 2h\xi^2(\lambda+\mu)(\Lambda+h) + \frac{5\mu^2+4\mu\lambda+\lambda^2}{\lambda+\mu}$$

Eqs. (2.32) and (2.33) together with Eq. (2.9) and (2.10) presents the complete elastic field of the layered system shown in Fig. 1. In the case of $\Lambda = 0$, the above solution reduces to the classical solution for an elastic layer [90]. It is noted that the surface effects are again solely represented by the parameter Λ appearing only in the terms A_1, B_1, C_1, D_1 and F. The first four terms vanish for a solid with no surface stress effects.

2.3 Solutions for a Semi-infinite Medium

Although a closed-form solution for the elastic field of a layer cannot be obtained due to the complexity of the integrals involved in the solution, the results of Sect. 2.2 can

be specialized for the case where h approaches infinity to obtain a set of closed-form solutions.

When h tends to infinity, the Eq. (2.20) together with Eq. (2.21) reduces to the following solutions.

$$A = \frac{\overline{p}(\xi)}{\xi^2} \tag{2.34}$$

$$B = \frac{\overline{p}(\xi)}{|\xi|}\frac{1+\frac{\lambda+\mu}{\lambda+2\mu}\Lambda|\xi|}{1+\Lambda|\xi|} + i\frac{\bar{t}(\xi)}{\xi}\frac{1}{1+\Lambda|\xi|} \tag{2.35}$$

$$C = D = 0 \tag{2.36}$$

In the case of a vertical point load of magnitude P,

$$\overline{p}(\xi) = P \tag{2.37}$$

and

$$A = \frac{P}{\xi^2};\ B = \frac{P}{|\xi|} - \frac{\mu}{\lambda+2\mu}\frac{P\Lambda}{1+\Lambda|\xi|} \tag{2.38}$$

If the surface stress effect is ignored, $\Lambda = 0$, the following closed-form solutions are obtained for stresses.

$$\begin{gathered}
(\sigma_{zz})_c = -\frac{2Pz^3}{\pi\left(z^2+x^2\right)^2};\quad (\sigma_{xx})_c = -\frac{2Pzx^2}{\pi\left(z^2+x^2\right)^2};\quad (\sigma_{xz})_c = -\frac{2Pz^2x}{\pi\left(z^2+x^2\right)^2} \\
(u_x)_c = \frac{P}{2\pi}\left(-\frac{1}{\lambda+\mu}\arctan\frac{x}{z} + \frac{z}{\mu}\frac{x}{x^2+z^2}\right) \\
(u_z)_c = \frac{P}{2\pi}\left(\frac{\lambda+2\mu}{\mu(\lambda+\mu)}\int_0^\infty \frac{e^{-\xi z}\cos(\xi x)}{\xi}d\xi + \frac{z}{\mu}\int_0^\infty e^{-\xi z}\cos(\xi x)\,d\xi\right)
\end{gathered} \tag{2.39}$$

where the subscript c is used to denote the classical solution in the absence of surface effects.

Note that based on Eq. (2.39) the stresses and vertical displacement show the classical R^{-1} $(R^2 = x^2 + z^2)$ and log R singularities. In addition, the displacement is indeterminate to within an arbitrary rigid body displacement due to the behavior of the first integral of the expression for $(u_z)_c$. The classical solutions given above are identical to the solutions given by Selvadurai [89].

For $\Lambda \neq 0$, the stress field of the half-plane can be expressed as,

$$\begin{aligned}
\sigma_{zz} &= (\sigma_{zz})_c + \frac{\mu P \Lambda}{\pi(\lambda + 2\mu)} z I_2(x,z) \\
\sigma_{xx} &= (\sigma_{xx})_c + \frac{\mu P \Lambda}{\pi(\lambda + 2\mu)} \left[2I_1(x,z) - z I_2(x,z) \right] \\
\sigma_{xz} &= (\sigma_{xz})_c - \frac{\mu P \Lambda}{\pi(\lambda + 2\mu)} \left[J_1(x,z) - z J_2(x,z) \right] \\
u_x &= (u_x)_c + \frac{P\Lambda}{2\pi} \left[\frac{1}{\lambda + \mu} J_0(x,z) - \frac{z}{\lambda + 2\mu} J_1(x,z) \right] \\
u_z &= (u_z)_c - \frac{P\Lambda}{2\pi} \left[\frac{\mu}{(\lambda + \mu)(\lambda + 2\mu)} I_0(x,z) + \frac{z}{\lambda + 2\mu} I_1(x,z) \right]
\end{aligned} \tag{2.40}$$

where

$$\begin{aligned}
I_0(x,z) &= \int_0^\infty \frac{e^{-\xi z} \cos(\xi x)}{1 + \Lambda \xi} d\xi = \frac{1}{2\Lambda} \left[e^{-\varphi} \mathrm{Ei}_1(\varphi) + e^{-\bar{\varphi}} \mathrm{Ei}_1(\bar{\varphi}) \right] \\
J_0(x,z) &= \int_0^\infty \frac{e^{-\xi z} \sin(\xi x)}{1 + \Lambda \xi} d\xi = \frac{i}{2\Lambda} \left[e^{-\varphi} \mathrm{Ei}_1(\varphi) - e^{-\bar{\varphi}} \mathrm{Ei}_1(\bar{\varphi}) \right] \\
I_1(x,z) &= -\frac{1}{\Lambda} \left[I_0 - \frac{z}{z^2 + x^2} \right] \\
J_1(x,z) &= -\frac{1}{\Lambda} \left[J_0 - \frac{x}{z^2 + x^2} \right] \\
I_2(x,z) &= -\frac{1}{\Lambda} \left[I_1 - \frac{z^2 - x^2}{(z^2 + x^2)^2} \right] \\
J_2(x,z) &= -\frac{1}{\Lambda} \left[J_1 - \frac{2xz}{(z^2 + x^2)^2} \right]
\end{aligned} \tag{2.41}$$

$$\varphi = \frac{1}{\Lambda}(z + ix); \quad \bar{\varphi} = \frac{1}{\Lambda}(z - ix) \tag{2.42}$$

and $\mathrm{Ei}_n(z)$ denotes the *Exponential Integral*.

It is found that the solution can be expressed in two parts to clearly identify the classical and non-classical parts. The characteristic length parameter Λ is found to control the non-classical terms associated with the surface energy effects. A close examination of the non-classical part of the solution given by Eqs. (2.40) and (2.41) shows that stresses contain a singularity of R^{-1} type and a resulting displacement has a logarithmic singularity at the loading point. However, it is important to note that the non-classical displacement is not indeterminate as in the case of the classical solution.

In the case of a horizontal point force of magnitude T applied at the origin of the coordinate system, eqns. (2.34) and (2.35) reduce to,

$$\text{A=0}, \qquad B = i\frac{T}{\xi}\frac{1}{1+\Lambda|\xi|} \tag{2.43}$$

Substitution of eqn. (2.43) in eqn. (2.7) and the evaluation of the resulting integrals yield,

$$\begin{aligned}
\sigma_{zz} &= (\sigma_{zz})_c + \frac{T\Lambda}{\pi} z J_2(x,z) \\
\sigma_{xx} &= (\sigma_{xx})_c - \frac{T\Lambda}{\pi}\left[z J_2(x,z) - 2J_1(x,z)\right] \\
\sigma_{xz} &= (\sigma_{xz})_c + \frac{T\Lambda}{\pi}\left[I_1(x,z) - z I_2(x,z)\right] \\
u_x &= (u_x)_c - \frac{T\Lambda}{2\pi}\left[\frac{\lambda+2\mu}{\mu(\lambda+\mu)} I_0(x,z) - \frac{z}{\mu} I_1(x,z)\right] \\
u_z &= (u_z)_c - \frac{T\Lambda}{2\pi}\left[\frac{1}{(\lambda+\mu)} J_0(x,z) + \frac{z}{\mu} J_1(x,z)\right]
\end{aligned} \tag{2.44}$$

where the classical elasticity solution corresponding to $\Lambda = 0$ is given by,

$$\begin{gathered}
(\sigma_{zz})_c = -\frac{2Txz^2}{\pi\left(z^2+x^2\right)^2};\ (\sigma_{xx})_c = -\frac{2Tx^3}{\pi\left(z^2+x^2\right)^2};(\sigma_{xz})_c = -\frac{2Tzx^2}{\pi\left(z^2+x^2\right)^2} \\
(u_z)_c = \frac{T}{2\pi}\left(\frac{1}{\lambda+\mu}\arctan\frac{x}{z} + \frac{z}{\mu}\frac{x}{x^2+z^2}\right)
\end{gathered} \tag{2.45}$$

$$\left(u_x\right)_c = \frac{T}{2\pi}\left(\frac{\lambda+2\mu}{\mu\left(\lambda+\mu\right)}\int_0^\infty \frac{e^{-\xi z}\cos\left(\xi x\right)}{\xi}d\xi - \frac{z}{\mu}\int_0^\infty e^{-\xi z}\cos\left(\xi x\right)d\xi\right)$$

The above classical elasticity solution has singularities similar to the vertical loading case discussed previously. In addition, the singularities of the non-classical part are also similar to the previous case.

For the axisymmetric problem, taking the limit *h* approaching infinity in eq. (2.32) results in,

$$A' = \frac{Z\left(\xi\right)}{2\xi^3}\frac{\lambda}{\left(\lambda+\mu\right)^2}\left[1+\frac{\mu}{\lambda}\xi\beta\left(\xi\right)\right] \tag{2.46}$$

$$B' = \frac{Z\left(\xi\right)}{2\xi^3}\frac{\xi}{\lambda+\mu}\left[1-\xi\beta\left(\xi\right)\right] \tag{2.47}$$

and

$$C' = D' = 0 \tag{2.48}$$

where

$$\beta\left(\xi\right) = \frac{\mu}{\left(\lambda+2\mu\right)}\frac{\Lambda}{1+\Lambda\xi} \tag{2.49}$$

By substituting the above solutions for the arbitrary functions in eqn. (2.9) the solution for a half-space can be obtained. In the case of a vertical point load of magnitude *P*, we have

$$Z\left(\xi\right) = -\frac{P}{2\pi} \tag{2.50}$$

The solution for elastic field can be written as

$$\begin{aligned}
\sigma_{rr} &= \left(\sigma_{rr}\right)_c + \frac{P}{2\pi}\left[\left(2I_2^0 - zI_3^0\right) - \frac{1}{r}\left(\frac{2\mu+\lambda}{\mu+\lambda}I_1^1 - zI_2^1\right)\right] \\
\sigma_{zz} &= \left(\sigma_{zz}\right)_c + \frac{P}{2\pi}zI_3^0 \\
\sigma_{\theta\theta} &= \left(\sigma_{\theta\theta}\right)_c + \frac{P}{2\pi}\left[\left(\frac{\lambda}{\mu+\lambda}\right)I_2^0 + \frac{1}{r}\left(\frac{2\mu+\lambda}{\mu+\lambda}I_1^1 - zI_2^1\right)\right]
\end{aligned} \tag{2.51}$$

$$\sigma_{rz} = \left(\sigma_{rz}\right)_c - \frac{P}{2\pi}\left(I_2^1 - zI_3^1\right)$$
$$u_r = \left(u_r\right)_c + \frac{P}{4\pi\mu}\left(\frac{2\mu+\lambda}{\mu+\lambda} I_1^1 - zI_2^1\right)$$
$$u_z = \left(u_z\right)_c - \frac{P}{4\pi\mu}\left(\frac{\mu}{\mu+\lambda} I_1^0 + zI_2^0\right)$$

where the classical solution for stresses and displacements denoted by a subscript 'c' is given by,

$$\left(\sigma_{rr}\right)_c = -\left(\frac{P}{2\pi}\right)\left\{\frac{3r^2 z}{\left(r^2+z^2\right)^{5/2}} - \frac{\mu}{\lambda+\mu}\left[\frac{1}{r^2} - \frac{z}{r^2\left(r^2+z^2\right)^{1/2}}\right]\right\}$$
$$\left(\sigma_{zz}\right)_c = -\left(\frac{P}{2\pi}\right)\frac{3z^3}{\left(r^2+z^2\right)^{5/2}}$$
$$\left(\sigma_{rz}\right)_c = -\left(\frac{P}{2\pi}\right)\frac{3rz^2}{\left(r^2+z^2\right)^{5/2}}$$

$$\left(\sigma_{\theta\theta}\right)_c = \left(\frac{P}{2\pi}\right)\left(\frac{\mu}{\lambda+\mu}\right)\left[\frac{z\left(2r^2+z^2\right)}{r^2\left(r^2+z^2\right)^{3/2}} - \frac{1}{r^2}\right] \tag{2.52}$$

$$\left(u_r\right)_c = \frac{P}{4\pi\mu}\left\{\frac{rz}{\left(r^2+z^2\right)^{3/2}} - \frac{\mu}{\lambda+\mu}\left[\frac{1}{r} - \frac{z}{r\left(r^2+z^2\right)^{1/2}}\right]\right\}$$
$$\left(u_z\right)_c = \frac{P}{4\pi\mu}\left\{\frac{z^2}{\left(r^2+z^2\right)^{3/2}} + \left(\frac{\lambda+2\mu}{\lambda+\mu}\right)\frac{1}{\left(r^2+z^2\right)^{1/2}}\right\}$$

and the integral I_n^m is defined as,

$$I_n^m\left(r,z\right) = \int_0^\infty \xi^n \beta\left(\xi\right) e^{-\xi z} J_m\left(\xi r\right) d\xi \tag{2.53}$$

It is noted that when the surface constant $\Lambda = 0$, I_n^m and the associated non-classical terms of Eqs. (2.51) vanish.

2.4 Numerical Results and Discussion

In this section, selected numerical results are presented to demonstrate the salient features of the elastic field. The surface elastic constants can be obtained from atomistic simulations [39, 45]. First, consider the case of an elastic half-plane subjected to vertical and horizontal point loads at the surface. The solution for the stress field is given in Sect. 2.3. A close examination of the present solutions indicates that it is convenient to introduce the non-dimensional coordinates, $x_0 = x/\Lambda$ and $z_0 = z/\Lambda$, and non-dimensionalize stresses by $2P/(\pi\Lambda)$ for the vertical loading case and by $2T/(\pi\Lambda)$ for the horizontal loading case. It can be shown that the non-dimensional stresses are only a function of the non-dimensional coordinates and the ratio λ/μ of the bulk material. In the present study, $\lambda/\mu = 2.226$ (e.g. Aluminum [91]) is used. The classical solution (in dimensional or nondimensional) is independent of Λ. However, the use of Λ in the nondimensionalization allows a comparison of the non-classical and classical solutions as shown in Figs. 2.2-2.7 but such comparison is valid for a fixed value of Λ and the results presented in this paper corresponds to a Al [1 1 1] surface $\Lambda = 0.15288$ *nm* [39].

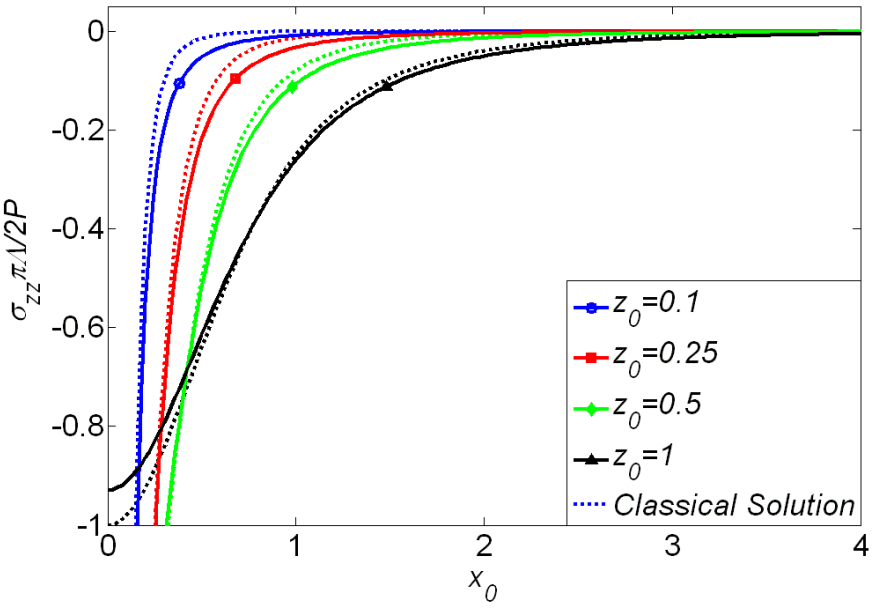

Fig. 2.2 Nondimensional vertical stress profiles at different depths due to a vertical point load.

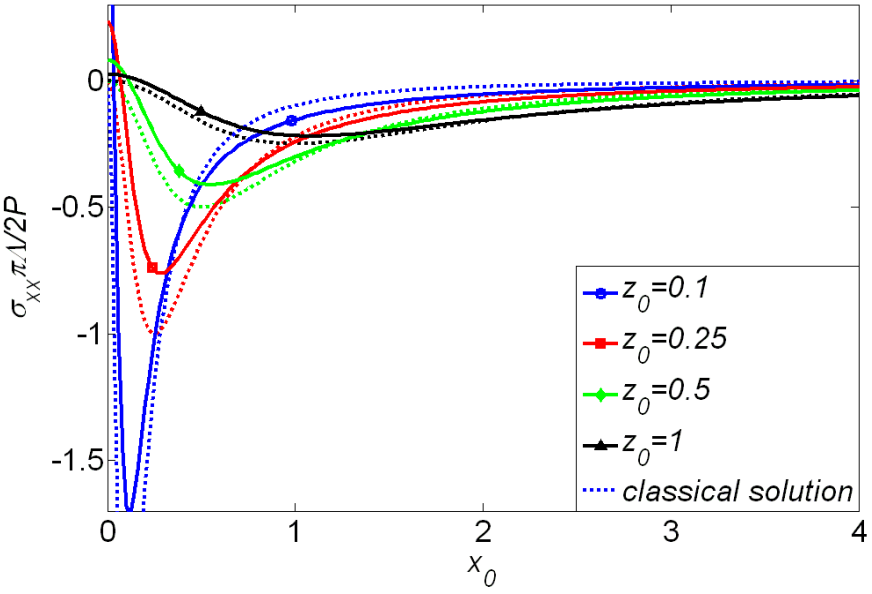

Fig. 2.3 Nondimensional horizontal stress profiles at different depths due to a vertical point load.

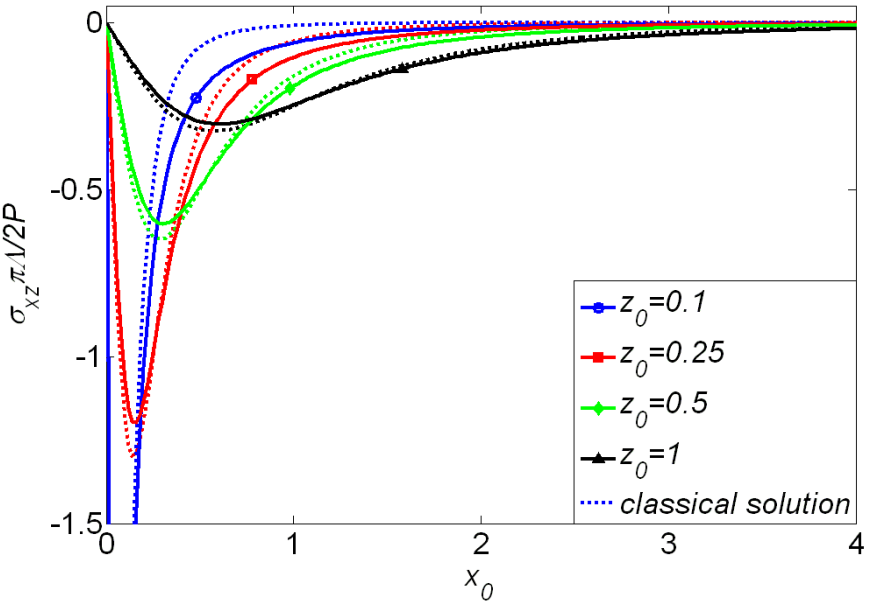

Fig. 2.4 Nondimensional shear stress profiles at different depths due to a vertical point load.

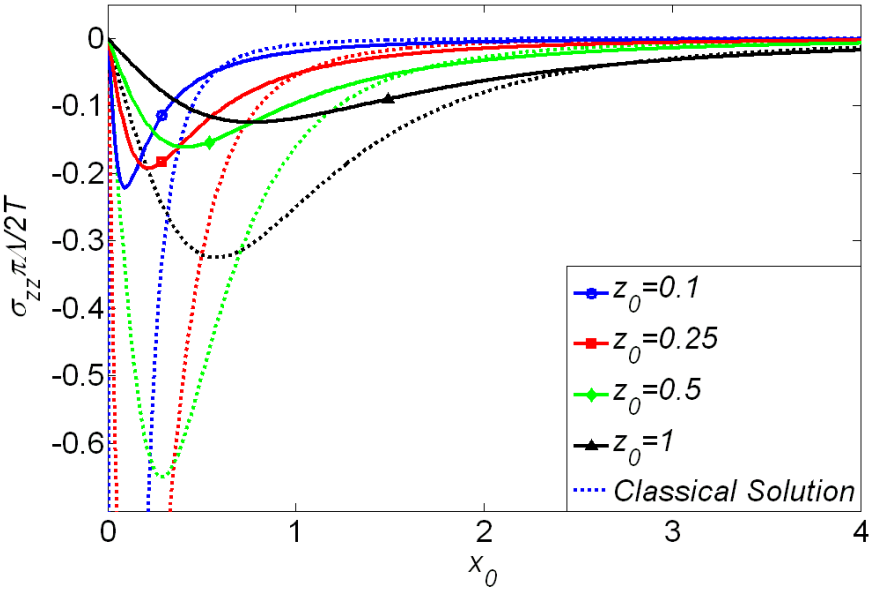

Fig. 2.5 Nondimensional vertical stress profiles at different depths due to a horizontal point load.

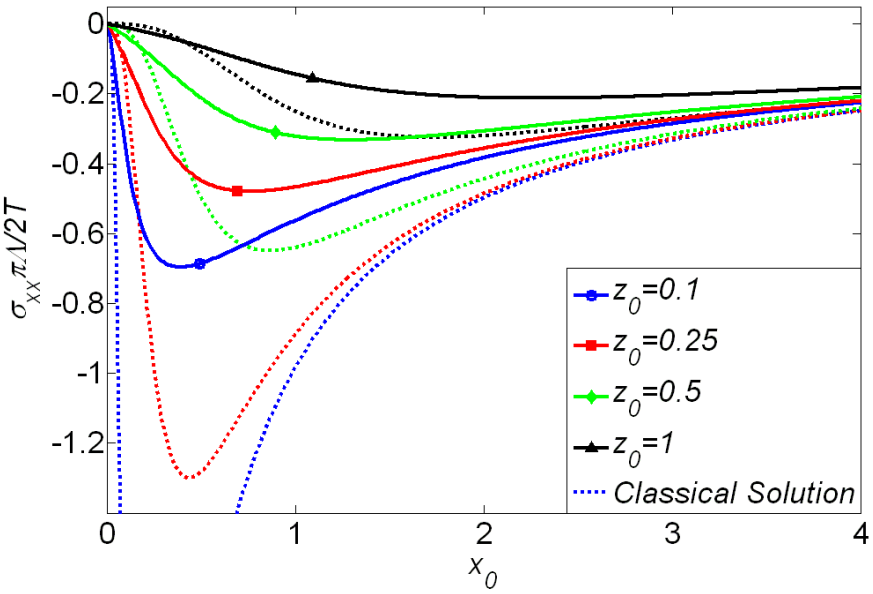

Fig. 2.6 Nondimensional horizontal stress profiles at different depths due to a horizontal point load.

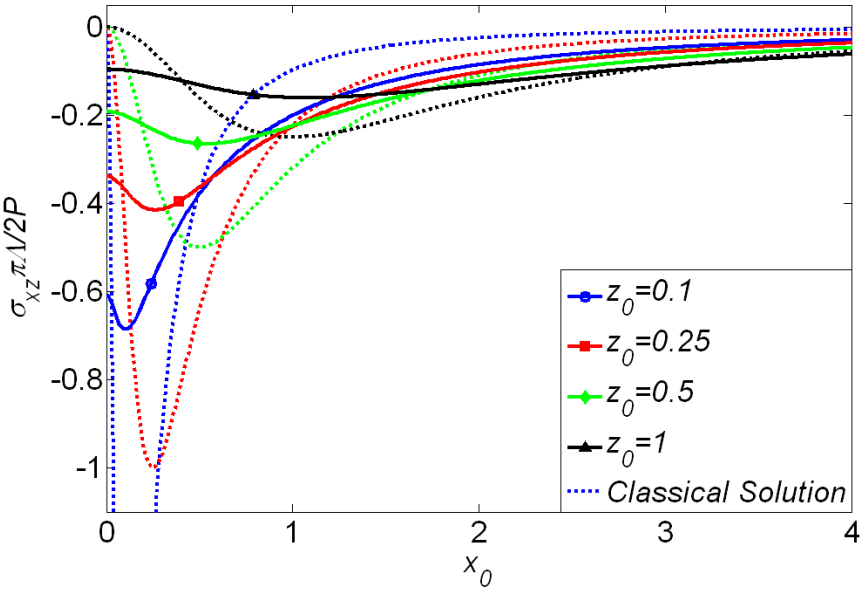

Fig. 2.7 Nondimensional shear stress profiles at different depths due to a horizontal point load.

Figs. 2.2-2.7 show the distribution along the *x*-direction of dimensionless vertical horizontal and shear stresses of a half-plane at different depths under vertical and horizontal point loads. Only the solutions along the positive *x*-axis are plotted due to the symmetry or anti-symmetry of the stress components. The broken lines denote the classical elasticity solution corresponding to $\kappa^s = 0$. It is clear that the influence of surface stresses is more significant under a horizontal load when compared to a vertical load. In the case of a vertical point load, the vertical normal stress has a negligible effect of surface stresses but the horizontal normal stress shows more visible influence. However, in the case of a horizontal point load, both vertical and horizontal normal stresses show a strong influence of the surface effects. This behaviour under different loading may be interpreted from eqns (2.11) and (2.12) by noting that eqn (2.11) is not modified from the classical case but eqn (2.12) contains the non-classical boundary condition associated with the surface stress effects. The zone of influence is confined primarily to $z_0 < 1.0$ for a vertical point load and $z_0 < 2.0$ for a horizontal load. Obviously, this behaviour is consistent with the expectation that the influence of surface effects would diminish with the distance from the surface. It should be noted that both σ_{xx} under

a vertical load and σ_{xz} under a horizontal load are no longer zero at the surface for $x_0 = 0$ due to the presence of surface tension. The results shown in Figs. 2.2-2.7 confirm that for materials like soft gels where the characteristic length (Λ) can be quite large or for nano-scale structures where Λ is comparable to material dimensions, the influence of surface effects need to be accounted.

Next consider the case of a three-dimensional elastic layer bonded to a rigid base and subjected to a uniformly distributed vertical load p_0 acting over a circular area of radius *a*. The solution for this axisymmetric problem is given in Sect 2.2. In this case, it is convenient to use the nondimensional coordinates, $r_0 = r/\Lambda$ and $z_0 = z/\Lambda$, a nondimensional layer thickness $h_0 = h/\Lambda$, and the radius of contact area $a_0 = a/\Lambda$. The solution appears in terms of semi-infinite integrals involving Bessel functions and was computed using numerical quadrature. The solutions for vertical and radial displacements of the surface of the layer along the r-axis are shown in Figs. 2.8 and 2.9 respectively for different layer thicknesses. Note that in the classical elasticity where there is no size effect, the elastic field can be uniquely determined by the value of h/a, but accounting for the surface effects, the elastic field is size-dependent. In the numerical results, we fixed the value of $a_0 = 10$. It can be seen from these figures that the surface effects have negligible influence on the vertical displacement profiles of the surface. Both the classical solution and the non-classical solution show similar effects of layer thickness; lower displacements as the layer thickness decreases. The influence of surface energy on the radial displacement profiles is quite significant. It is clear that the magnitudes of displacements are smaller than that in classical solution, which implies the surface stress effects suppress the deformation and stiffen the surface.

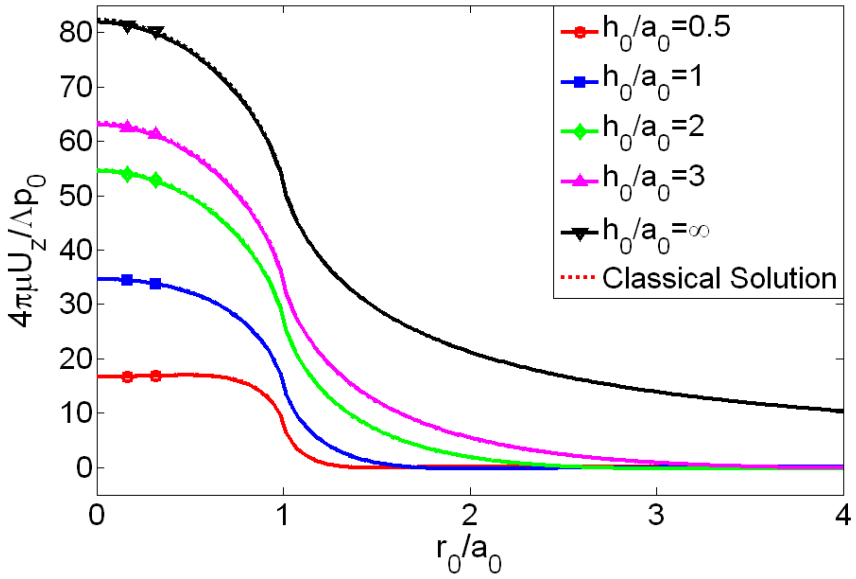

Fig. 2.8 Vertical displacement of layer surface due to a uniformly distributed vertical load.

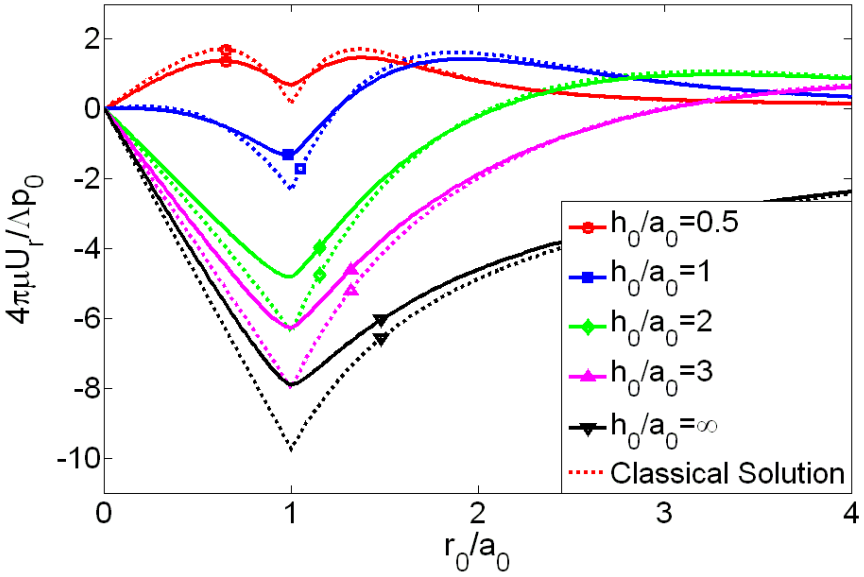

Fig. 2.9 Radial displacement of layer surface due to a uniformly distributed vertical load.

The nondimensional stress components of the layer at different depths are plotted in Figs. 2.10– 2.13. The layer thickness, $h_0 = 3a_0 = 30$. It is found that the influence of surface effects on vertical stress profiles is quite negligible similar to the solutions shown in Fig. 2.2, however, the surface effects have an influence on the other stress components

as shown in Fig. 2.11-2.13, and the zone of influence is about $r_0 / a_0 = 1.5$. The influence of surface effects tends to decrease as r or z increases which is in accordance with the expectation that the surface effects primarily affect the region near the surface and loading zone. The discontinuity of σ_{rr} at the loading edge $r_0 / a_0 = 1$ may be caused by the errors of numerical quadrature when computing the semi-infinite integrals.

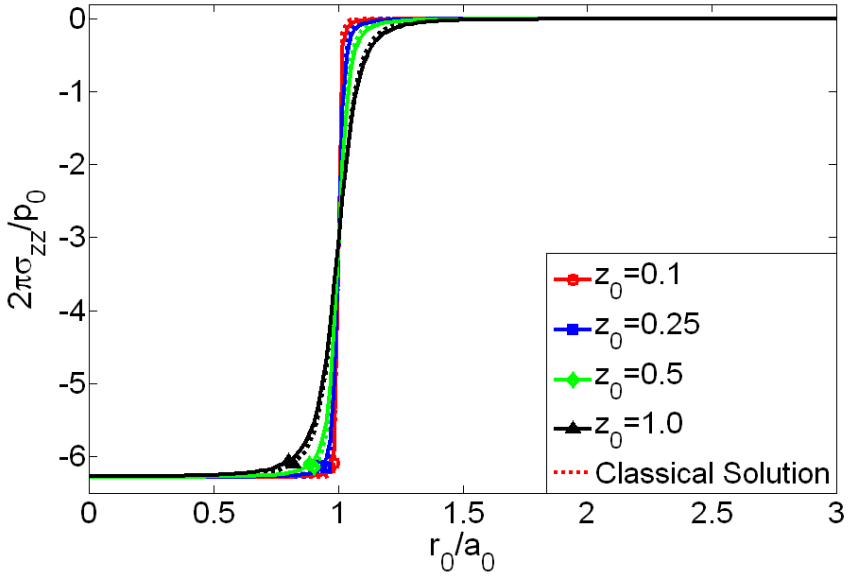

Fig. 2.10 Radial distribution of vertical stress due to a uniformly distributed vertical load.

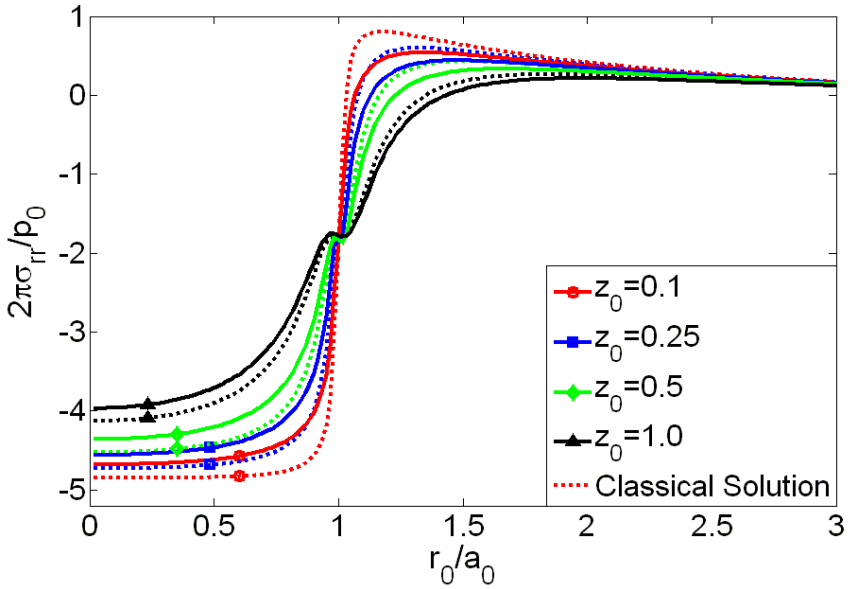

Fig. 2.11 Radial distribution of radial stress due to a uniformly distributed vertical load.

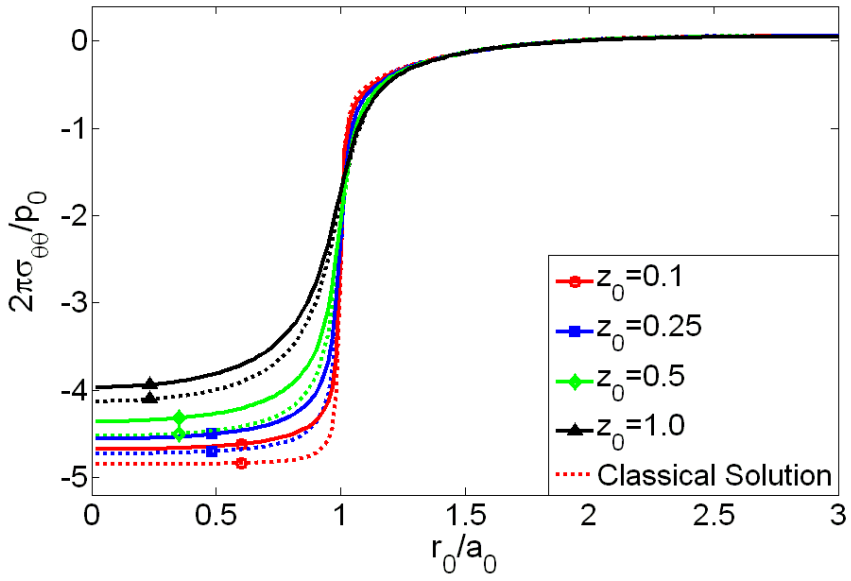

Fig. 2.12 Radial distribution of hoop stress due to a uniformly distributed vertical load.

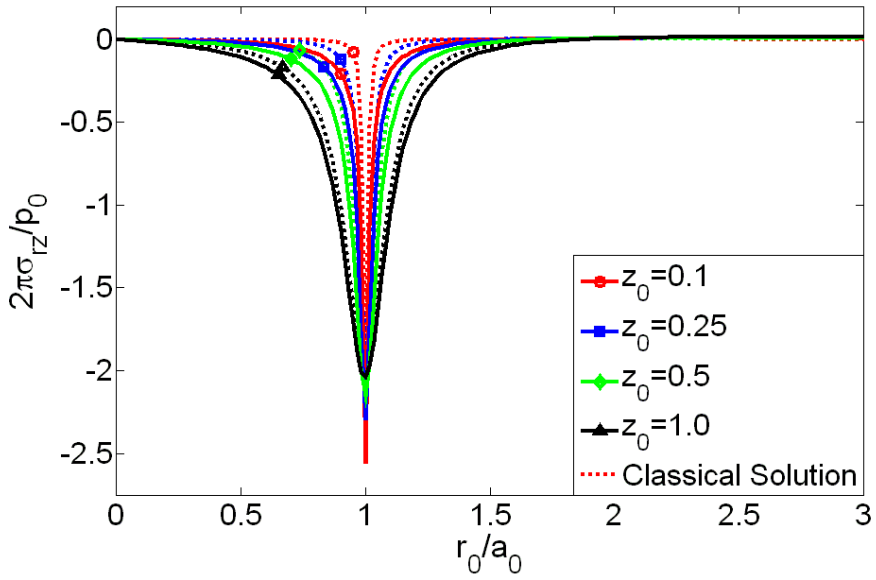

Fig. 2.13 Radial distribution of shear stress due to a uniformly distributed vertical load.

Chapter 3

ELASTIC FIELD OF A NANO-FILM SUBJECTED TO TANGENTIAL SURFACE LOAD: ASYMMETRIC PROBLEM

3.1 Problem Description

In this chapter, general three-dimensional problems for an isotropic elastic thin layer bonded to a rigid substrate and subjected to surface tangential loading is considered in the presence of surface stresses (Fig. 3.1). Similar to Chapter 2, the Gurtin-Murdoch continuum theory is used to consider the surface energy effects. This class of problems has important applications in the study of nanocoatings, nanotribology and surface formations in soft elastic solids. Unlike the layer problems considered in Chapter 2, the deformation and stress field under tangential loading is three dimensional consisting of three components of displacements and six independent stresses. In this study, cylindrical coordinates are employed and the loading is assumed to apply over a circular area. This allows the formulation of the present class of problems by using Fourier expansion in the θ-direction and Hankel integral transforms in the radial direction.

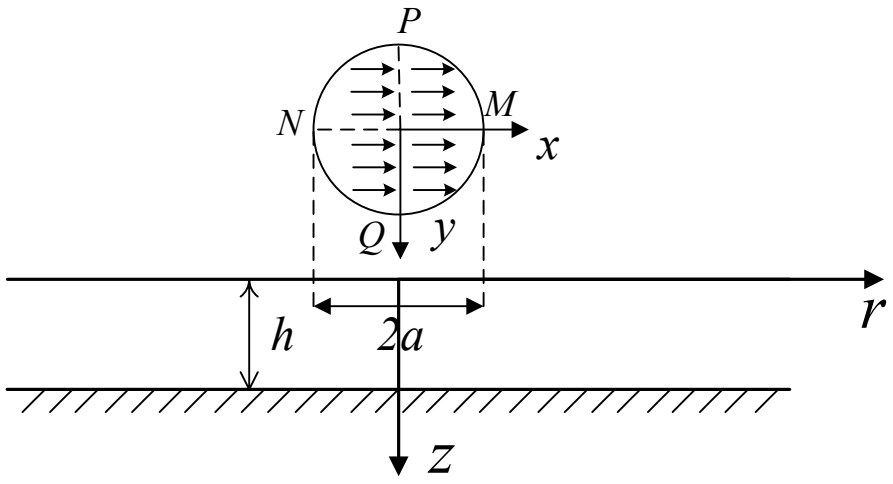

Fig. 3.1 Elastic layer subjected to tangential surface loading.

Muki [87] presented a powerful general solution based on Hankel integral transforms to solve three-dimensional boundary-value problems in classical elasticity. In this chapter, Muki's method is extended to solve problems involving thin layers subjected to tangential loading in the presence of surface energy effects.

3.2 General Solution of Elastic Field

According to Muki [87], the general solution for the displacement and stress components of an isotropic homogeneous elastic solid can be expressed with respect to a cylindrical coordinate system (r,θ,z) as,

$$u_r = \frac{1}{2}\sum_{m=0}^{\infty}\left[U_{m+1}(r,z) - V_{m-1}(r,z)\right]\cos m\theta \tag{3.1}$$

$$u_\theta = \frac{1}{2}\sum_{m=0}^{\infty}\left[U_{m+1}(r,z) + V_{m-1}(r,z)\right]\sin m\theta \tag{3.2}$$

$$\begin{aligned} u_z = -\sum_{m=0}^{\infty}\int_0^{\infty}\Bigg\{&\left[A_m\xi + \left(\frac{2\mu}{\lambda+\mu} + z\xi\right)B_m\right]e^{-\xi z} \\ &+\left[C_m\xi - \left(\frac{2\mu}{\lambda+\mu} - z\xi\right)D_m\right]e^{\xi z}\Bigg\}\xi^2 J_m(\xi r)\cos m\theta\, d\xi \end{aligned} \tag{3.3}$$

$$\begin{aligned} \frac{\sigma_{rr}}{2\mu} = \sum_{m=0}^{\infty}\Bigg[&\int_0^{\infty}\Bigg\{\left[-A_m\xi + \left(\frac{2\lambda+\mu}{\lambda+\mu} - z\xi\right)B_m\right]e^{-\xi z} \\ &+\left[C_m\xi + \left(\frac{2\lambda+\mu}{\lambda+\mu} + z\xi\right)D_m\right]e^{\xi z}\Bigg\}\xi^3 J_m(\xi r)\,d\xi \\ &-\frac{(m+1)}{2r}U_{m+1} - \frac{(m-1)}{2r}V_{m-1}\Bigg]\cos m\theta \end{aligned} \tag{3.4}$$

$$\begin{aligned} \frac{\sigma_{\theta\theta}}{2\mu} = \sum_{m=0}^{\infty}\Bigg[&\frac{\lambda}{\lambda+\mu}\int_0^{\infty}\left(B_m e^{-\xi z} + D_m e^{\xi z}\right)\xi^3 J_m(\xi r)\,d\xi \\ &+\frac{(m+1)}{2r}U_{m+1} + \frac{(m-1)}{2r}V_{m-1}\Bigg]\cos m\theta \end{aligned} \tag{3.5}$$

$$\frac{\sigma_{zz}}{2\mu}=\sum_{m=0}^{\infty}\Bigg[\int_0^{\infty}\Bigg\{\Bigg[A_m\xi+\left(\frac{\mu}{\lambda+\mu}+z\xi\right)B_m\Bigg]e^{-\xi z} -\Bigg[C_m\xi-\left(\frac{\mu}{\lambda+\mu}-z\xi\right)D_m\Bigg]e^{\xi z}\Bigg\}\xi^3 J_m(\xi r)\,d\xi\Bigg]\cos m\theta \tag{3.6}$$

$$\frac{\sigma_{r\theta}}{2\mu}=\sum_{m=0}^{\infty}\Bigg[\int_0^{\infty}\left(E_m e^{-\xi z}+F_m e^{\xi z}\right)\xi^3 J_m(\xi r)\,d\xi -\frac{(m+1)}{2r}U_{m+1}+\frac{(m-1)}{2r}V_{m-1}\Bigg]\sin m\theta \tag{3.7}$$

$$\frac{\sigma_{\theta z}}{2\mu}=\frac{1}{2}\sum_{m=0}^{\infty}\left(L_{m+1}+K_{m-1}\right)\sin m\theta\,;\quad \frac{\sigma_{zr}}{2\mu}=\frac{1}{2}\sum_{m=0}^{\infty}\left(L_{m+1}-K_{m-1}\right)\cos m\theta \tag{3.8}$$

where μ and λ denote the Lamé constants; and

$$\begin{aligned}U_{m+1}(r,z)&=\int_0^{\infty}\Big\{\left[-A_m\xi+(1-z\xi)B_m+2E_m\right]e^{-\xi z}\\&\qquad+\left[C_m\xi+(1+z\xi)D_m+2F_m\right]e^{\xi z}\Big\}\xi^2 J_{m+1}(\xi r)\,d\xi\\V_{m-1}(r,z)&=\int_0^{\infty}\Big\{\left[-A_m\xi+(1-z\xi)B_m-2E_m\right]e^{-\xi z}\\&\qquad+\left[C_m\xi+(1+z\xi)D_m-2F_m\right]e^{\xi z}\Big\}\xi^2 J_{m-1}(\xi r)\,d\xi\end{aligned} \tag{3.9}$$

$$\begin{aligned}L_{m+1}(r,z)&=\int_0^{\infty}\Bigg\{\Bigg[A_m\xi-\left(\frac{\lambda}{\lambda+\mu}-z\xi\right)B_m-E_m\Bigg]e^{-\xi z}\\&\qquad+\Bigg[C_m\xi+\left(\frac{\lambda}{\lambda+\mu}+z\xi\right)D_m+F_m\Bigg]e^{\xi z}\Bigg\}\xi^3 J_{m+1}(\xi r)\,d\xi\\K_{m-1}(r,z)&=\int_0^{\infty}\Bigg\{\Bigg[A_m\xi-\left(\frac{\lambda}{\lambda+\mu}-z\xi\right)B_m+E_m\Bigg]e^{-\xi z}\\&\qquad+\Bigg[C_m\xi+\left(\frac{\lambda}{\lambda+\mu}+z\xi\right)D_m-F_m\Bigg]e^{\xi z}\Bigg\}\xi^3 J_{m-1}(\xi r)\,d\xi\end{aligned} \tag{3.10}$$

The arbitrary functions A_m, B_m, C_m, D_m, E_m and F_m appearing in Eqs. (3.3)-(3.10) can be determined from the boundary conditions.

Equations (3.1)-(3.10) are applicable only to situations where the applied loading is symmetric about $\theta=0$ (x-axis). Under more general loading, the above solutions should

contain the complete Fourier expansion with respect to θ including the anti-symmetric terms of θ. The anti-symmetric terms can be easily obtained by replacing $\cos m\theta \to \sin m\theta$ and $\sin m\theta \to -\cos m\theta$ [87].

3.3 Boundary-value Problem

Following boundary conditions can be established at the top surface of the layer by using the generalized Young-Laplace equation.

$$\frac{\partial \sigma_{rr}^{s}}{\partial r} + \frac{1}{r}\frac{\partial \sigma_{r\theta}^{s}}{\partial \theta} + \frac{\sigma_{rr}^{s} - \sigma_{\theta\theta}^{s}}{r} + \sigma_{rz}\big|_{z=0} + g(r,\theta) = 0 \tag{3.11}$$

$$\frac{\partial \sigma_{\theta r}^{s}}{\partial r} + \frac{1}{r}\frac{\partial \sigma_{\theta\theta}^{s}}{\partial \theta} + \frac{2\sigma_{r\theta}^{s}}{r} + \sigma_{\theta z}\big|_{z=0} + f(r,\theta) = 0 \tag{3.12}$$

$$\sigma_{zz}\big|_{z=0} = 0 \tag{3.13}$$

where $g(r,\theta)$ and $f(r,\theta)$ denote the applied surface tractions in the radial and circumferential directions respectively; and a superscript '*s*' is used to represent the surface stress components.

The layer is perfectly bonded to a rigid substrate at the bottom and the boundary conditions are,

$$u_r\big|_{z=h} = 0\,; \quad u_\theta\big|_{z=h} = 0\,; \quad u_z\big|_{z=h} = 0 \tag{3.14}$$

Neglecting the displacement gradient term, the surface constitutive relations can be expressed as [40, 41],

$$\sigma_{\beta\alpha}^{s} = \tau^{s}\delta_{\beta\alpha} + 2\left(\mu^{s} - \tau^{s}\right)\varepsilon_{\beta\alpha} + \left(\lambda^{s} + \tau^{s}\right)\varepsilon_{\gamma\gamma}\delta_{\beta\alpha} \tag{3.15}$$

where μ^{s} and λ^{s} are surface Lamé constants and τ^{s} is the residual surface tension under unstrained conditions.

The loading functions $g(r,\theta)$ and $f(r,\theta)$ can be expressed in the following general form.

$$f\left(r,\theta\right) = \sum_{m=0}^{\infty}\left[p_m(r)\sin m\theta - p'_m(r)\cos m\theta\right] \tag{3.16}$$

$$g(r,\theta)=\sum_{m=0}^{\infty}\left[q_m(r)\sin m\theta+q'_m(r)\cos m\theta\right]$$

In the ensuing analysis, $p'_m=q'_m=0$ in view of the fact that only loading symmetric about $\theta=0$ is considered in the current formulation. As mentioned previously, the solutions corresponding to the anti-symmetric loading terms involving p'_m and q'_m can be obtained from the symmetric solutions by replacing $\cos m\theta\rightarrow\sin m\theta$, $\sin m\theta\rightarrow-\cos m\theta$, $p_m\rightarrow p'_m$ and $q_m\rightarrow q'_m$. In addition, it is convenient to obtain solutions corresponding to a single value of m without loss of generality.

Considering only a single value of m and applying Hankel integral transforms to Eqs. (3.11)-(3.13) together with the substitution of Eqs. (3.1)- (3.10), result in the following set of equations to determine the arbitrary functions appearing in the general solution.

$$-\left(\Lambda_1\xi+1\right)A_m\xi+\left(\Lambda_1\xi+\frac{\lambda}{\lambda+\mu}\right)B_m+\left(\Lambda_1\xi-1\right)C_m\xi+\left(\Lambda_1\xi-\frac{\lambda}{\lambda+\mu}\right)D_m=\frac{1}{2\mu}\frac{X_m+Y_m}{2\xi^2} \tag{3.17}$$

$$\frac{\mu}{\lambda+\mu}\left(B_m+D_m\right)+\left(A_m-C_m\right)\xi=0 \tag{3.18}$$

$$\left[\frac{\lambda-\mu}{\lambda+\mu}B_m-2\left(A_m+B_mh\right)\xi\right]e^{-\xi h}+\frac{\lambda+3\mu}{\lambda+\mu}D_me^{\xi h}=0 \tag{3.19}$$

$$\frac{\lambda+3\mu}{\lambda+\mu}B_me^{-\xi h}+\left[\frac{\lambda-\mu}{\lambda+\mu}D_m+2\left(C_m+D_mh\right)\xi\right]e^{\xi h}=0 \tag{3.20}$$

$$\left(\Lambda_2\xi+1\right)E_m+\left(\Lambda_2\xi-1\right)F_m=-\frac{1}{2\mu}\frac{X_m-Y_m}{2\xi^2} \tag{3.21}$$

$$E_me^{-\xi h}+F_me^{\xi h}=0 \tag{3.22}$$

where

$$\Lambda_1=\frac{\lambda+2\mu}{2\mu\left(\lambda+\mu\right)}\left(2\mu^s+\lambda^s-\tau^s\right);\ \Lambda_2=\frac{\mu^s-\tau^s}{\mu} \tag{3.23}$$

and $$X_m = \int_0^\infty \left[p_m(r) - q_m(r) \right] r J_{m-1}(\xi r)\, dr \,;\; Y_m = \int_0^\infty \left[p_m(r) + q_m(r) \right] r J_{m+1}(\xi r)\, dr \quad (3.24)$$

The parameters Λ_1 and Λ_2 represent the ratios of surface to bulk elastic properties and have a dimension of length. The functions X_m and Y_m are related to Hankel integral transforms of applied loads.

The solution of Eqs. (3.17)-(3.22) yields,

$$\begin{aligned}
A_m &= \frac{1}{4\mu}\frac{A_t}{H_t}\frac{X_m + Y_m}{2\xi^3}; \qquad B_m = \frac{1}{4\mu}\frac{B_t}{H_t}\frac{X_m + Y_m}{2\xi^2} \\
C_m &= \frac{1}{4\mu}\frac{C_t}{H_t}\frac{X_m + Y_m}{2\xi^3}; \qquad D_m = \frac{1}{4\mu}\frac{D_t}{H_t}\frac{X_m + Y_m}{2\xi^2} \\
E_m &= \frac{1}{2\mu}\frac{1}{E_t}\frac{X_m - Y_m}{2\xi^2}; \qquad F_m = \frac{1}{2\mu}\frac{1}{F_t}\frac{X_m - Y_m}{2\xi^2}
\end{aligned} \quad (3.25)$$

where

$$\begin{aligned}
A_t &= -\frac{\mu}{\lambda+\mu}\left[\frac{3\lambda+5\mu}{\lambda+\mu} + 2\xi h + \frac{2(\lambda+\mu)}{\mu}\xi^2 h^2 + \frac{\lambda+3\mu}{\lambda+\mu} e^{2\xi h} \right] \\
B_t &= \frac{\lambda+3\mu}{\lambda+\mu} e^{2\xi h} + (1 + 2\xi h) \\
C_t &= -\frac{\mu}{\lambda+\mu}\left[\frac{3\lambda+5\mu}{\lambda+\mu} - 2\xi h + \frac{2(\lambda+\mu)}{\mu}\xi^2 h^2 + \frac{\lambda+3\mu}{\lambda+\mu} e^{-2\xi h} \right] \\
D_t &= -\left[\frac{\lambda+3\mu}{\lambda+\mu} e^{-2\xi h} + (1 - 2\xi h) \right] \\
E_t &= \left(e^{-2\xi h} - 1 \right)\Lambda_2 \xi - \left(e^{-2\xi h} + 1 \right) \\
F_t &= \left(e^{2\xi h} - 1 \right)\Lambda_2 \xi + \left(e^{2\xi h} + 1 \right)
\end{aligned} \quad (3.26)$$

$$H_t = \frac{\lambda+3\mu}{\lambda+\mu}\left[\cosh(2\xi h) + \Lambda_1 \xi \sinh(2\xi h) \right] + 2h\xi^2(\lambda+\mu)(\Lambda_1 + h) + \frac{\lambda^2 + 4\lambda\mu + 5\mu^2}{(\lambda+\mu)^2}$$

The complete elastic field of the layer can be obtained by substituting the above solutions for arbitrary functions into Eqs. (3.1) - (3.10). It can be seen that the parameters Λ_i (i=1, 2) associated with the surface elastic properties appear only in E_t, F_t and H_t. Note that Λ_i vanish in the absence of surface stress effects and the above solutions reduce to the classical elasticity solutions.

In the following analysis, the above solution is specialized for two common loading cases relevant to practical applications. First, consider the case where the layer is subjected to a uniformly distributed tangential traction of intensity p_0 along the x-direction over a circular area with radius a as shown in Fig. 3.1. In view of Eqn. (3.16) ,

$$\begin{aligned} f(r,\theta) &= \sum_{m=0}^{\infty} p_m(r)\sin m\theta = \begin{cases} -p_0\sin\theta & r \le a \\ 0 & r > a \end{cases} \\ g(r,\theta) &= \sum_{m=0}^{\infty} q_m(r)\cos m\theta = \begin{cases} p_0\cos\theta & r \le a \\ 0 & r > a \end{cases} \end{aligned} \tag{3.27}$$

Therefore,

$$p_m(r) = \begin{cases} -p_0 & m=1 \\ 0 & m \ne 1 \end{cases}; \quad q_m(r) = \begin{cases} p_0 & m=1 \\ 0 & m \ne 1 \end{cases} \tag{3.28}$$

Substitution of Eqn. (3.28) into Eqn. (3.24) yields,

$$\begin{aligned} X_m &= \begin{cases} -2p_0\dfrac{aJ_1(\xi a)}{\xi} & m=1 \\ 0 & m \ne 1 \end{cases} \\ Y_m &= 0 \end{aligned} \tag{3.29}$$

If h approaches infinity, the solution for a layer can be specialized to obtain the solution for a semi-infinite domain. In the case of a semi-infinite medium, the Eq. (3.25) together with Eq. (3.26) reduces to the following solutions for arbitrary functions.

$$A_m = -\frac{1}{4(\lambda+\mu)\xi^3}\frac{X_m + Y_m}{1+\Lambda_1\xi} \tag{3.30}$$

$$B_m = -\frac{1}{4\mu\xi^2}\frac{X_m + Y_m}{1+\Lambda_1\xi} \tag{3.31}$$

$$E_m = -\frac{1}{4\mu\xi^2}\frac{X_m - Y_m}{1+\Lambda_2\xi} \tag{3.32}$$

$$C_m = D_m = F_m = 0 \tag{3.33}$$

In the case of a point load of magnitude Q in the x-direction, Eq. (3.29) reduces to,

$$X_m = \begin{cases} -\dfrac{Q}{\pi} & m = 1 \\ 0 & m \neq 1 \end{cases} \tag{3.34}$$

$Y_m = 0$ for all m

If the surface stress effects are ignored, i.e. $\Lambda_i = 0$ ($i=1, 2$), the following closed-form solutions are obtained for the case of a tangential point load.

$$\begin{aligned}
\left(u_r\right)_c &= \frac{Q}{4\pi\mu\rho}\left[\frac{\mu}{\lambda+\mu}\frac{z}{\left(\rho+z\right)} + 2 - \frac{z^2}{\rho^2}\right]\cos\theta \\
\left(u_\theta\right)_c &= \frac{Q}{4\pi\mu\rho}\left[\frac{\mu}{\lambda+\mu}\frac{z}{\left(\rho+z\right)} - \frac{\lambda+2\mu}{\lambda+\mu}\right]\sin\theta \\
\left(u_z\right)_c &= \frac{Q}{4\pi\mu\rho}\left[\frac{\mu}{\lambda+\mu}\frac{r}{\left(\rho+z\right)} + \frac{zr}{\rho^2}\right]\cos\theta
\end{aligned} \tag{3.35}$$

$$\begin{aligned}
\left(\sigma_{rr}\right)_c &= -\frac{Q}{2\pi\rho}\left[\frac{2r}{\rho^2} - \frac{3rz^2}{\rho^4} + \frac{1}{r}\frac{\rho-z}{\rho+z}\left(\frac{\mu}{\lambda+\mu} + \frac{2z}{\rho} + \frac{z^2}{\rho^2}\right)\right]\cos\theta \\
\left(\sigma_{\theta\theta}\right)_c &= -\frac{Q}{2\pi\rho}\left[\frac{\mu}{\lambda+\mu}\frac{r}{\rho^2} - \frac{1}{r}\frac{\rho-z}{\rho+z}\left(\frac{\mu}{\lambda+\mu} + \frac{2z}{\rho} + \frac{z^2}{\rho^2}\right)\right]\cos\theta \\
\left(\sigma_{zz}\right)_c &= -\frac{3Qrz^2}{2\pi\rho^5}\cos\theta \\
\left(\sigma_{r\theta}\right)_c &= \frac{Q}{2\pi\rho}\left[\frac{r}{\rho^2} - \frac{1}{r}\frac{\rho-z}{\rho+z}\left(\frac{\mu}{\lambda+\mu} + \frac{2z}{\rho} + \frac{z^2}{\rho^2}\right)\right]\sin\theta
\end{aligned} \tag{3.36}$$

$$\left(\sigma_{\theta z}\right)_c = \frac{Q}{2\pi\rho}\left[\frac{z}{\rho^2} - \frac{2r^2 z - z^3}{\rho^4}\right]\sin\theta$$

$$\left(\sigma_{zr}\right)_c = -\frac{Qz}{\pi\rho^3}\cos\theta$$

where the subscript '*c*' is used to denote the classical solution in the absence of surface effects and

$$\rho = \sqrt{r^2 + z^2} \tag{3.37}$$

Note that Eqs. (3.35) and (3.36) are identical to the classical elasticity solution [87].

For $\Lambda_i \neq 0$, the elastic field of a half space under a tangential point load can be expressed as,

$$\begin{aligned}
u_r &= \left(u_r\right)_c + \frac{Q}{4\pi\mu}\left[\frac{\mu}{\lambda+\mu}\frac{I_1^2 - I_1^0}{2} - \frac{z}{2}\left(I_2^2 - I_2^0\right) - \frac{2}{r}J_0^1\right]\cos\theta \\
u_\theta &= \left(u_\theta\right)_c + \frac{Q}{4\pi\mu}\left[\frac{1}{r}\left(\frac{\mu}{\lambda+\mu}I_0^1 - zI_1^1\right) - \left(J_1^2 - J_1^0\right)\right]\sin\theta \\
u_z &= \left(u_z\right)_c - \frac{Q}{4\pi\mu}\left[\frac{\mu}{\lambda+\mu}I_1^1 + zI_2^1\right]\cos\theta
\end{aligned} \tag{3.38}$$

and the stresses are given by,

$$\begin{aligned}
\sigma_{rr} &= \left(\sigma_{rr}\right)_c + \frac{Q}{2\pi}\left[2I_1^1 - zI_2^1 - \frac{1}{r}\left(\frac{\lambda}{\lambda+\mu}I_1^2 - zI_2^2 - 2J_1^2\right)\right]\cos\theta \\
\sigma_{\theta\theta} &= \left(\sigma_{\theta\theta}\right)_c + \frac{Q}{2\pi}\left[\frac{\lambda}{\lambda+\mu}I_2^1 + \frac{1}{r}\left(\frac{\lambda}{\lambda+\mu}I_1^2 - zI_2^2 - 2J_1^2\right)\right]\cos\theta \\
\sigma_{zz} &= \left(\sigma_{zz}\right)_c + \frac{Qz}{2\pi}I_3^1\cos\theta \\
\sigma_{r\theta} &= \left(\sigma_{r\theta}\right)_c - \frac{Q}{2\pi}\left[J_2^1 + \frac{1}{r}\left(\frac{\lambda}{\lambda+\mu}I_1^2 - zI_2^2 - 2J_1^2\right)\right]\sin\theta
\end{aligned} \tag{3.39}$$

$$\sigma_{\theta z} = \left(\sigma_{\theta z}\right)_c - \frac{Q}{2\pi}\left[\frac{1}{r}\left(I_1^1 - zI_1^2\right) - \frac{J_2^2 - J_2^0}{2}\right]\sin\theta$$

$$\sigma_{zr} = \left(\sigma_{zr}\right)_c + \frac{Q}{2\pi}\left[\frac{1}{r}J_1^1 + \frac{I_2^0 - I_2^2}{2} + \frac{z}{2}\left(I_3^2 - I_3^0\right)\right]$$

where

$$I_n^m\left(r,z\right) = \int_0^\infty \frac{\Lambda_1\xi^n}{1+\Lambda_1\xi}e^{-\xi z}J_m\left(\xi r\right)d\xi\,;\, J_n^m\left(r,z\right) = \int_0^\infty \frac{\Lambda_2\xi^n}{1+\Lambda_2\xi}e^{-\xi z}J_m\left(\xi r\right)d\xi \qquad (3.40)$$

The non-classical part of the above solution is a function of the characteristic length parameters Λ_i (*i=1, 2*) associated with the surface energy effects. If $\Lambda_i = 0$, the two integrals I_n^m and J_n^m vanish and the solution obviously reduces to the classical elasticity solution.

3.3 Numerical Results and Discussion

The analytical solutions for a layer under tangential loading expressed in terms of semi-infinite integrals cannot be evaluated analytically to obtain a closed form solution due to the complexity of the integrands. Numerical integration techniques are therefore employed to calculate the elastic field of a layer. In this section, selected numerical results are presented to elucidate the influence of surface tension and surface elastic constants on the elastic field. Following Chapter 2, the non-dimensional coordinates $r_0 = r/\Lambda_1$ and $z_0 = z/\Lambda_1$, non-dimensional layer thickness $h_0 = h/\Lambda_1$, and loading radius $a_0 = a/\Lambda_1$ are introduced. The material surface constants are, μ^s=1.655 N/m, λ^s=-1.247 N/m, τ^s=-0.1154 N/m corresponding to Nickel [1 1 1] surface [45], the bulk elastic constants for Nickel are: μ=76.0 GPa and λ =126.1 [91]. The radius of loading area is set to $a_0 = 10$.

Figs. 3.2-3.4 show the distribution of the surface displacements of the layer due to a uniformly distributed tangential load. Only the solutions at selected cross sections, for example, $\theta = 0$ or $\theta = \pi/2$, are plotted along the radial direction, in that the solutions

along the θ-direction show a sine or cosine distribution (Eq. (3.1) - (3.8)). It is found that the surface stress effects have a quite strong influence on the displacement profiles and make the layer stiffer than the classical case. Both the classical and the non-classical solutions show similar influence of the layer thickness such that displacements decrease with decreasing layer thickness.

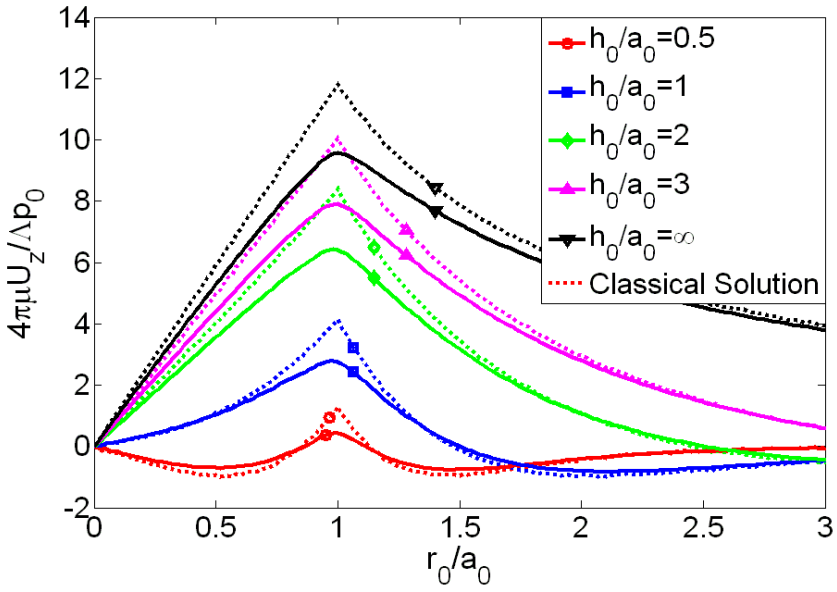

Fig. 3.2 Non-dimensional vertical displacement at the surface of a layer due to a tangential distributed load ($\theta = 0$).

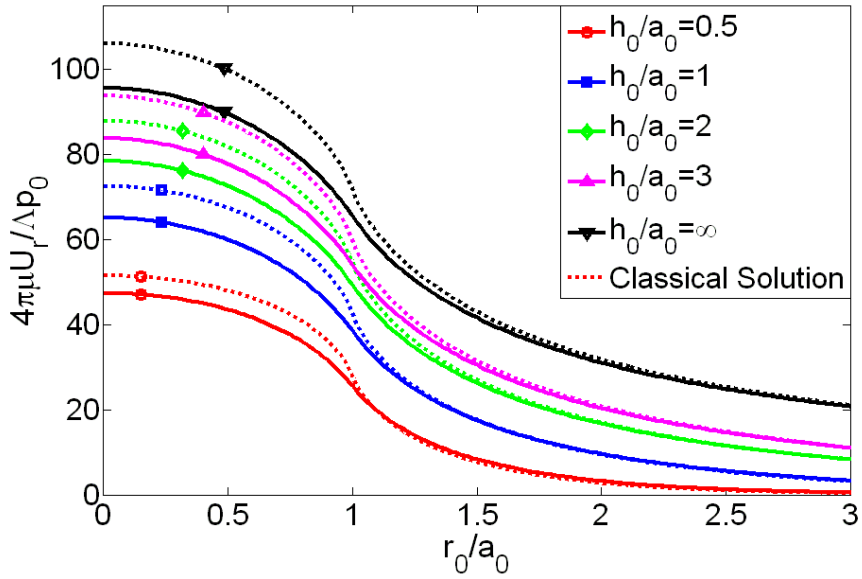

Fig. 3.3 Non-dimensional radial displacement at the surface of a layer due to a tangential distributed load ($\theta = 0$).

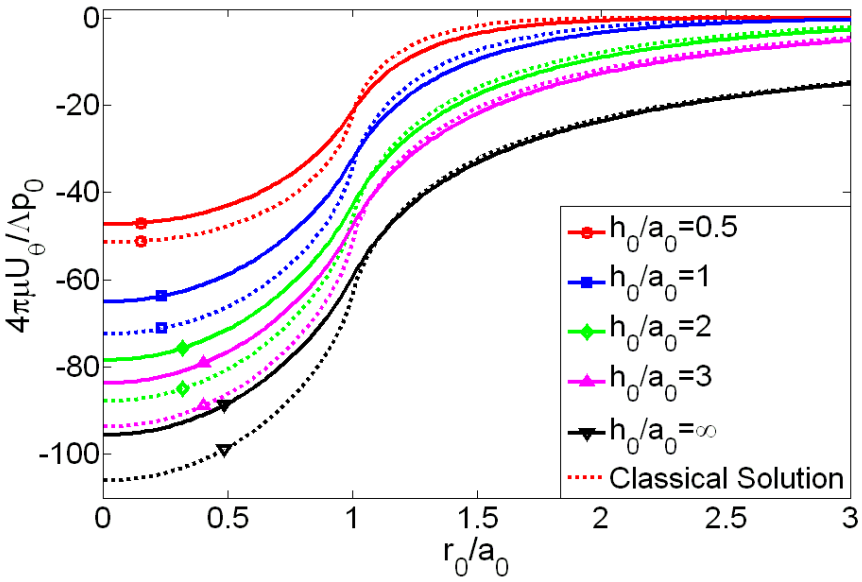

Fig. 3.4 Non-dimensional circumferential displacement of the surface of a layer due to tangential distributed load ($\theta = \frac{\pi}{2}$).

Figs. 3.5-3.8 show the distribution of stresses of a layer at different depths under a uniformly distributed tangential loading. It can be clearly seen from these figures that the

influence of surface effect is quite significant on the stress field. The radius of influence is confined to 1.5 times the contact radius. The consideration of surface stresses lead to lower bulk stresses in all cases of layer thickness which is consistent with the stiffening behavior observed previously for displacements.

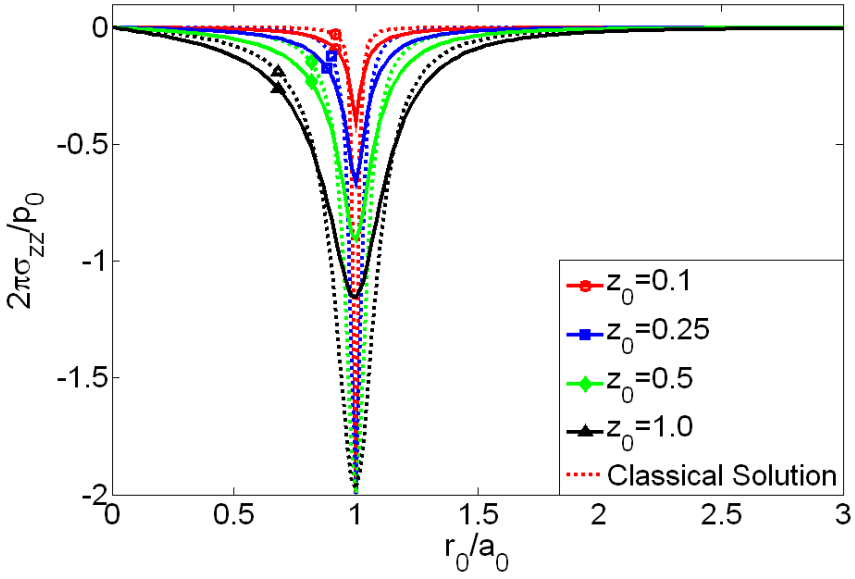

Fig. 3.5 Non-dimensional stress σ_{zz} of a layer due to tangential load ($\theta = 0$).

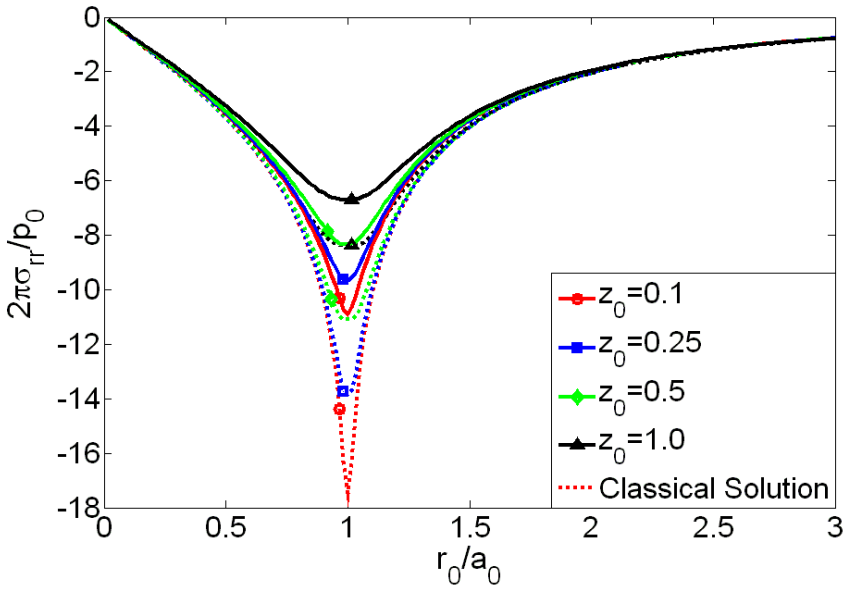

Fig. 3.6 Non-dimensional stress σ_{rr} of a layer due to tangential load ($\theta = 0$).

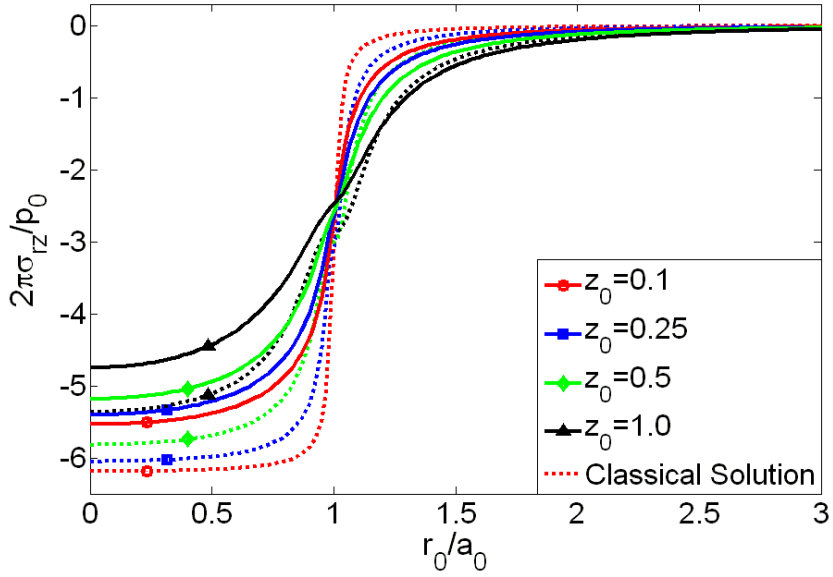

Fig. 3.7 Non-dimensional stress σ_{rz} of a layer due to tangential load ($\theta = 0$).

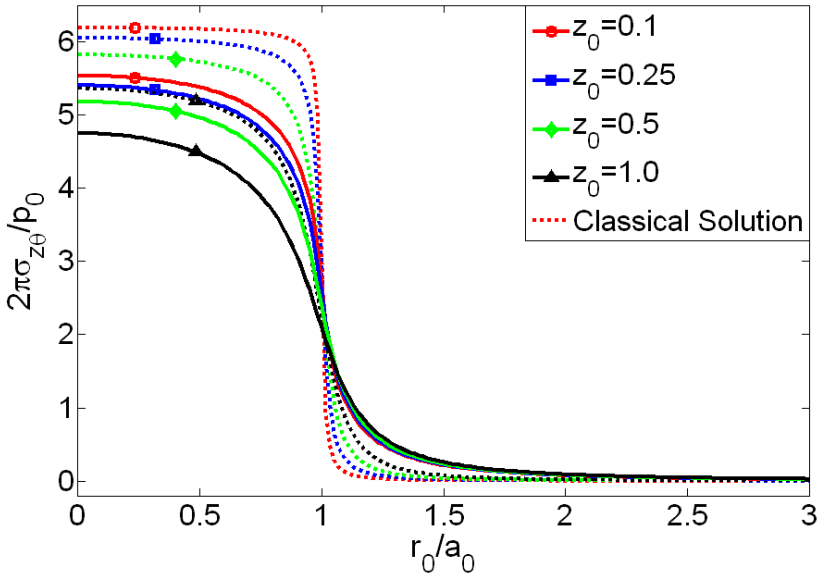

Fig. 3.8 Non-dimensional stress $\sigma_{\theta z}$ of a layer due to tangential load ($\theta = \frac{\pi}{2}$).

Next consider the shear stresses at the interface of the film/substrate, which is an important factor in the delamination of the film from substrate. Interfacial shear stress components σ_{rz} and $\sigma_{\theta z}$ along the *r*-direction are shown in Fig. 3.9 and 3.10,

respectively. It can be seen that the influence of the surface effects is more significant for relatively thin layers when compared to thick ones, since the influence of surface stresses is confined to vicinity of the surface and has little effect on the base of the layer if it is not closer to the surface.

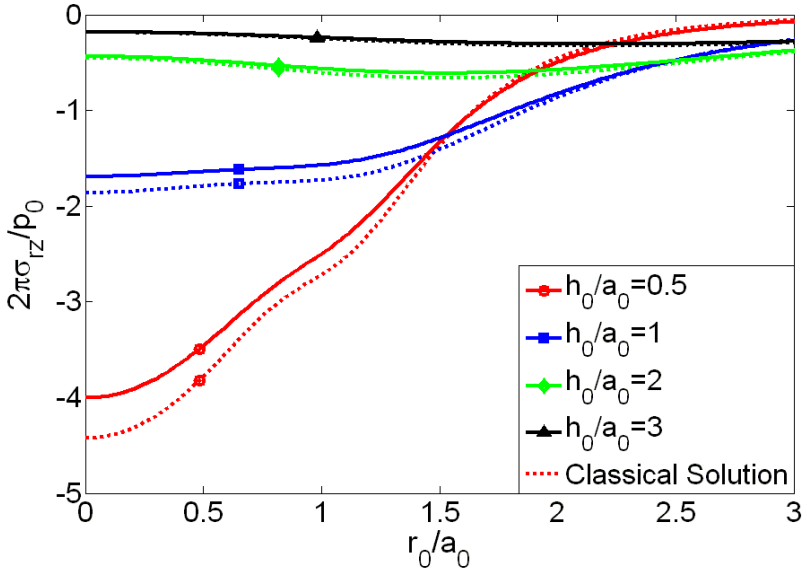

Fig. 3.9 Non-dimensional stress σ_{rz} at the interface of film/substrate ($\theta = 0$).

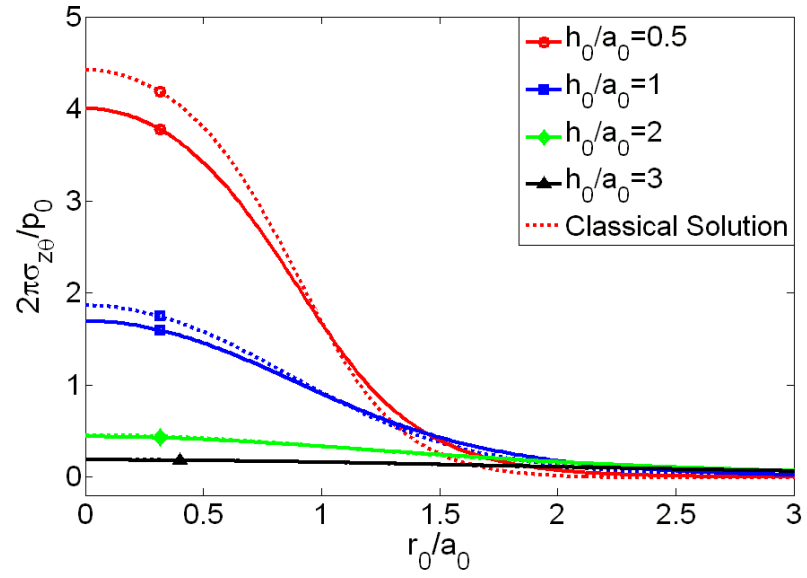

Fig. 3.10 Non-dimensional stress $\sigma_{\theta z}$ at the interface of film/substrate ($\theta = \frac{\pi}{2}$).

Chapter 4

RIGID INDENTATION OF AN ELASTIC SEMI-INFINITE SOLID

4.1 Problem Description

In this chapter, indentation of an isotropic elastic half space by a rigid body is considered. The surface energy effects are taken into account by using the Gurtin-Murdoch continuum model. According to author's knowledge, the influence of surface energy effects on indentation problems has not been investigated in the past and such effects could have important implications on the mechanics of nanoindentation and contact mechanics of soft solids. Consider a semi-infinite elastic solid indented by an axisymmetric rigid punch as shown in Fig. 4.1. The radius of contact area and indentation depth are denoted by a and d respectively. The solutions for elastic field caused by flat-ended cylindrical, conical and spherical rigid indenters are derived in this chapter. Selected numerical results are presented to demonstrate the salient features of the elastic field and vertical stiffness and the influence of surface energy effects.

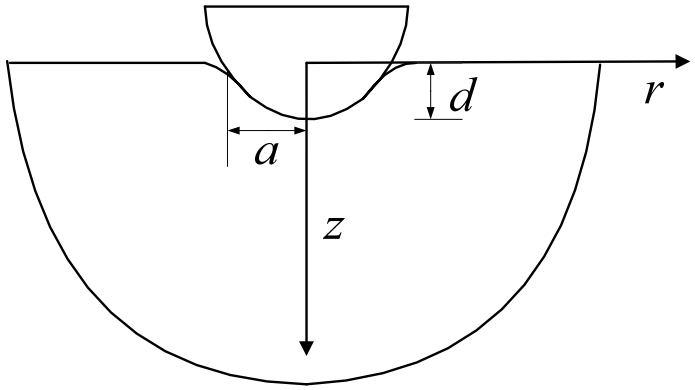

Fig. 4.1 Elastic half space indented by an axi-symmetric rigid body.

4.2 Formulation of the Elastic Field

The solution of axisymmetric contact problem shown in Fig. 4.1 can be formulated by using a cylindrical coordinate system (r, θ, z) and general solutions for

axisymmetric deformations given by Eq. (2.9) and (2.10) in Chapter 2. Since the thickness of the medium is infinite, the arbitrary functions *C'* and *D'* appearing in Eq (2.9) and (2.10) are set to zero to ensure the regularity of displacements and stresses as z approaches infinity. Note that u_θ vanishes due to the axial symmetry and all non-zero field variables are independent of θ. Accordingly, the general solutions for displacements and stresses for an isotropic half space can be expressed as,

$$u_r = \frac{\lambda+\mu}{\mu}\int_0^\infty \xi^2\left[-A\xi+(1-z\xi)B\right]e^{-\xi z}J_1(\xi r)\,d\xi \tag{4.1}$$

$$u_z = -\frac{\lambda+\mu}{\mu}\int_0^\infty \xi^2\left[A\xi+\left(\frac{2\mu}{\lambda+\mu}+z\xi\right)B\right]e^{-\xi z}J_0(\xi r)\,d\xi \tag{4.2}$$

$$\begin{aligned}\frac{\sigma_{rr}}{2(\lambda+\mu)} = &\int_0^\infty \xi^3\left[-A\xi+\left(\frac{2\lambda+\mu}{\mu+\lambda}-z\xi\right)B\right]e^{-\xi z}J_0(\xi r)\,d\xi \\ &-\frac{1}{r}\int_0^\infty \xi^2\left[-A\xi+(1-z\xi)B\right]e^{-\xi z}J_1(\xi r)\,d\xi\end{aligned} \tag{4.3}$$

$$\frac{\sigma_{\theta\theta}}{2(\lambda+\mu)} = \frac{\lambda}{\mu+\lambda}\int_0^\infty \xi^3 B e^{-\xi z}J_0(\xi r)\,d\xi+\frac{1}{r}\int_0^\infty \xi^2\left[-A\xi+(1-z\xi)B\right]e^{-\xi z}J_1(\xi r)\,d\xi \tag{4.4}$$

$$\frac{\sigma_{zz}}{2(\lambda+\mu)} = \int_0^\infty \xi^3\left[A\xi+\left(\frac{\mu}{\mu+\lambda}+z\xi\right)B\right]e^{-\xi z}J_0(\xi r)\,d\xi \tag{4.5}$$

$$\frac{\sigma_{rz}}{2(\lambda+\mu)} = \int_0^\infty \xi^3\left[A\xi-\left(\frac{\lambda}{\mu+\lambda}-z\xi\right)B\right]e^{-\xi z}J_1(\xi r)\,d\xi \tag{4.6}$$

where λ and μ are Lame constants of the bulk material; $J_n(\xi)$ denotes the *n*-th order Bessel Function of the first kind; and the arbitrary functions A and B are to be determined from the boundary conditions.

The mixed boundary conditions corresponding to the indentation problem shown in Fig. 4.1 can be expressed as,

$$u_z\big|_{z=0} = d - \delta\left(\frac{r}{a}\right) \qquad 0 \le r \le a \tag{4.7}$$

$$\sigma_{zz}\big|_{z=0} = 0 \qquad a < r < \infty \tag{4.8}$$

$$\sigma_{rz}\big|_{z=0} = -\kappa^s \left(\frac{d^2 u_r}{dr^2} + \frac{1}{r}\frac{du_r}{dr} - \frac{u_r}{r^2} \right)_{z=0} \tag{4.9}$$

in which the function $\delta(r/a)$ is related to the profiles of indenter and was defined by Sneddon [75]. Note that the parameters *d* and *a* are unspecified yet.

The Eq. (4.9) must be true for all values of *r* at the surface and substitution of Eq. (4.1) and Eq. (4.6) into Eq. (4.9) results in,

$$\left(1 + \Lambda_0 \xi\right) A\xi = \left(\frac{\lambda}{\lambda + \mu} + \Lambda_0 \xi \right) B \tag{4.10}$$

where $\Lambda_0 = \kappa^s / 2\mu$.

Substitution of Eq. (4.2) and (4.5) in Eq. (4.7) and (4.8) together with Eq. (4.10) results in,

$$-\int_0^\infty \xi^2 \left[\frac{(\lambda + 2\mu) + (\lambda + 3\mu)\Lambda_0 \xi}{\mu(1 + \Lambda_0 \xi)} \right] B J_0(\xi r) d\xi = d - \delta\left(\frac{r}{a}\right) \qquad 0 \le r \le a \tag{4.11}$$

$$\int_0^\infty \xi^3 \left[\frac{(\lambda + \mu) + (\lambda + 2\mu)\Lambda_0 \xi}{\mu(1 + \Lambda_0 \xi)} \right] B J_0(\xi r) d\xi = 0 \qquad a < r < \infty \tag{4.12}$$

Introduce,

$$M(\xi) = \xi^2 \left[\frac{(\lambda + 2\mu) + (\lambda + 3\mu)\Lambda_0 \xi}{\mu(1 + \Lambda_0 \xi)} \right] B \tag{4.13}$$

$$\frac{\alpha \xi M(\xi)}{1 - g(\xi)} = \xi^3 \left[\frac{(\lambda + \mu) + (\lambda + 2\mu)\Lambda_0 \xi}{\mu(1 + \Lambda_0 \xi)} \right] B \tag{4.14}$$

where α is an arbitrary constant to be determined.

In view of Eqs. (4.13) and (4.14), Eqs. (4.11) and (4.12) reduces to the following dual integral equation system.

$$\int_0^\infty M(\xi) J_0(\xi r) d\xi = f(r) \qquad 0 \le r \le a \tag{4.15}$$

$$\int_0^\infty \frac{\xi M(\xi)}{1-g(\xi)} J_0(\xi r) d\xi = 0 \qquad a < r < \infty \tag{4.16}$$

where

$$f(r) = -\left[d - \delta\left(\frac{r}{a}\right) \right] \tag{4.17}$$

The solution of dual integral equations of the type (4.15) and (4.16) has been studied by Lebedev and Ufliand [76], and Noble [92]. Following Lebedev and Ufliand [76], introduce the solutions as

$$M(\xi) = \left[1 - g(\xi)\right] \int_0^a \phi(t) \cos(\xi t)\, d\xi \tag{4.18}$$

where the function $g(\xi)$ can be determined from Eq. (4.13) and (4.14) as,

$$g(\xi) = 1 - \frac{(\lambda + 2\mu) + (\lambda + 3\mu)\Lambda_0 \xi}{(\lambda + \mu) + (\lambda + 2\mu)\Lambda_0 \xi} \alpha \tag{4.19}$$

and the function $\phi(t)$ is the solution of the following Fredholm Integral Equation of the second kind.

$$\phi(t) - \frac{1}{\pi} \int_0^a \phi(x) \left[K(x+t) + K(x-t) \right] dx = F(t) \qquad 0 \le t \le a \tag{4.20}$$

where

$$F(t) = \frac{2}{\pi} \left[f(0) + t \int_0^{\frac{\pi}{2}} f'(t \sin\theta) d\theta \right] \tag{4.21}$$

$$K(x) = \int_0^\infty g(\xi) \cos(\xi x)\, d\xi \tag{4.22}$$

Note that, to ensure the convergence of the kernel function $K(x)$, i.e. $g(\xi)\to 0$, as $\xi\to\infty$,

$$\alpha=\frac{\lambda+2\mu}{\lambda+3\mu} \tag{4.23}$$

From Eq. (4.5), the distribution of normal stress under the punch can be expressed as:

$$\sigma_{zz}\big|_{z=0}=\frac{2\mu(\lambda+2\mu)}{\lambda+3\mu}\left[\frac{\phi(a)}{\sqrt{a^2-r^2}}-\int_r^a\frac{\phi'(t)\,dt}{\sqrt{t^2-r^2}}\right]\qquad r<a \tag{4.24}$$

Now introduce the following relations to simplify the ensuing derivation.

$$\begin{aligned}&\Lambda=\Lambda_0\frac{\lambda+2\mu}{\lambda+\mu}=\frac{\kappa^s(\lambda+2\mu)}{2\mu(\lambda+\mu)}\\&\tau=\frac{t}{a}\qquad y=\frac{x}{a}\qquad a_0=\frac{a}{\Lambda}\qquad \phi(t)=\frac{2}{\pi}dH(\tau)\end{aligned} \tag{4.25}$$

Eq. (4.19) yields

$$g(\xi)=-\frac{\mu^2}{(\lambda+\mu)(\lambda+3\mu)}\frac{1}{1+\Lambda\xi} \tag{4.26}$$

and the Fredholm Integral Equation (4.20) reduces to,

$$H(\tau)-\frac{1}{\pi}\int_0^1 H(y)\big[G(y+\tau)+G(y-\tau)\big]dy=F_0(\tau)\qquad 0\le\tau\le 1 \tag{4.27}$$

where

$$G(u)=\frac{\mu^2 a_0}{(\lambda+\mu)(\lambda+3\mu)}\big[\sin(a_0u)\,\mathrm{si}(a_0u)+\cos(a_0u)\,\mathrm{ci}(a_0u)\big] \tag{4.28}$$

and si(x) and ci(x) are sine and cosine integrals defined by

$$\begin{aligned}&\mathrm{si}(x)=\int_0^x\frac{\sin t}{t}dt-\frac{\pi}{2}\\&\mathrm{ci}(x)=-\int_x^\infty\frac{\cos t}{t}dt=\int_0^x\frac{\cos t-1}{t}dt+\ln(x)+c\end{aligned} \tag{4.29}$$

Here c is Euler's constant with the value of 0.577215664...

The function $F_0(\tau)$ of the right-hand side of Eq. (4.27) can be obtained from Eq. (4.17) and (4.21) as given below.

(a) For a flat-ended cylindrical indenter with radius *a*

$$\begin{aligned} &\delta\left(\frac{r}{a}\right)=0 && 0\le r\le a \\ &F_0(\tau)=-1 \end{aligned} \tag{4.30}$$

(b) For a conical indenter with an apex angle 2θ

$$\begin{aligned} &\delta\left(\frac{r}{a}\right)=r\cot\theta && 0\le r\le a \\ &F_0(\tau)=-\left(1-\frac{\pi a}{2d}\tau\cot\theta\right) \end{aligned} \tag{4.31}$$

(c) For a spherical indenter with radius *R*

$$\begin{aligned} &\delta\left(\frac{r}{a}\right)=R\left(1-\sqrt{1-\frac{r^2}{R^2}}\right) && 0\le r\le a \\ &F_0(\tau)=-\left(1-\frac{a^2}{dR}\tau^2\right) && (a\ll R) \end{aligned} \tag{4.32}$$

The Fredholm Integral Equation of the second kind (eq. (4.27)) can be solved numerically. If the solution of $H(\tau)$ is known, the functions *A* and *B* can be determined from Eq. (4.10), (4.13), (4.14), (4.18), (4.25) and (4.26), so that the complete elastic field can be obtained.

Note that when $\Lambda=0$, Eq. (4.26) becomes a constant and

$$g(\xi)=-\frac{\mu^2}{(\lambda+\mu)(\lambda+3\mu)} \tag{4.33}$$

The dual integral equations (4.15) and (4.16) in this case become

$$\int_0^\infty M(\xi) J_0(\xi r) d\xi = f(r) \qquad (0 \le r \le a) \tag{4.34}$$

$$\int_0^\infty \xi M(\xi) J_0(\xi r) d\xi = 0 \qquad (a < r < \infty) \tag{4.35}$$

which corresponds to the classical indentation problem of a half space in the absence of surface energy effects that was solved by Sneddon [75].

From Eq. (4.24), a simple expression can be obtained for the magnitude of the total applied force on the indenter. Integrating the normal stress under the indenter over the area of the contact region yields,

$$P = -\frac{8\mu(\lambda + 2\mu)}{\lambda + 3\mu} da \int_0^1 H(\tau) d\tau \tag{4.36}$$

In the case of a flat-ended cylindrical indenter that has a sharp corner, the stress is singular at the edge. However, if the indenter has a smooth profile, for example, the conical and spherical indenters, the continuity of normal stress around the circle $r = a$ $(\tau = 1)$ gives an additional equation

$$\phi(a) = H(1) = 0 \tag{4.37}$$

which can be used together with equation (4.27) to set up the relationships between the penetration depth *d* and the radius of contact area *a* for the conical and spherical indenters.

For convenience, introduce a dimensionless parameter γ as

$$\gamma = \frac{a}{a_c} \tag{4.38}$$

where a_c is the radius of contact area corresponding to a homogeneous half space in the classical case, and the relationship between a_c and indentation depth *d* were obtained by Sneddon [75] as:

(a) For a flat-ended cylindrical indenter

$$a_c = a \tag{4.39}$$

(b) For a conical indenter

$$d = \frac{1}{2}\pi a_c \tan\theta \tag{4.40}$$

(c) For a spherical tip indenter

$$a_c = \sqrt{Rd} \qquad \left(a_c \ll R\right) \tag{4.41}$$

Accordingly, the function $F_0(\tau)$ in Eq. (4.30)-(4.32) can be rewritten as follows

(a) Flat ended punch

$$F_0(\tau) = -1 \tag{4.42}$$

(b) Conical indenter

$$F_0(\tau) = -(1-\gamma\tau) \tag{4.43}$$

(c) Spherical indenter

$$F_0(\tau) = -\left(1-\gamma^2\tau^2\right) \qquad \left(a \ll R\right) \tag{4.44}$$

The formulation of the problem is now complete for each type of indenter considered. It can be seen from the Fredholm Integral equation (4.27) that the right-hand function $F_0(\tau)$ is solely related to the indenter profile and the kernel function $G(u)$ that is related to the boundary conditions depends on the surface energy effects.

4.3 Numerical Results and Discussion

Selected numerical results are presented in this section and the surface elastic constants can be obtained from atomistic simulation [39, 45], but they can be for arbitrary materials in the present study, because nondimensional coordinates $r_0 = r/\Lambda$, $a_0 = a/\Lambda$ and $d_0 = d/\Lambda$ are used in the solution. For the bulk material, assuming Aluminum,

$\lambda = 58.17\,\text{GPa}$ and $\mu = 26.13\,\text{GPa}$ [91]. The Fredholm Integral Equation of the second kind (4.27) can be solved numerically. It should be pointed out that the ratio γ is equal to 1 for the flat ended cylindrical indenter, but it is unspecified for conical and spherical indenters. In the present calculations for conical and spherical indenters, first set the parameter γ equal to 1 and then iterate until a proper value is obtained such that $H(1) = 0$. Then the updated values are used to solve the Fredholm Integral Equation (4.27) and obtain the numerical solution of function $H(\tau)$.

Fig. 4.2 shows the relationships between parameter γ and the radius of contact area for different indenter shapes. It is interesting that it shows a size-dependent behavior due to the influence of surface energy effects. It can be seen that γ is lower than 1, which means that the contact area is smaller than that in the classical case. When the radius of contact area is small, the material becomes stiffer. It seems that the influence on the contact area is only limited to less than 1% and can be neglected in the indentation test. However, for some soft materials such as polymer gels and biological materials whose intrinsic characteristic lengths are large, the influence of surface effect may be prominent.

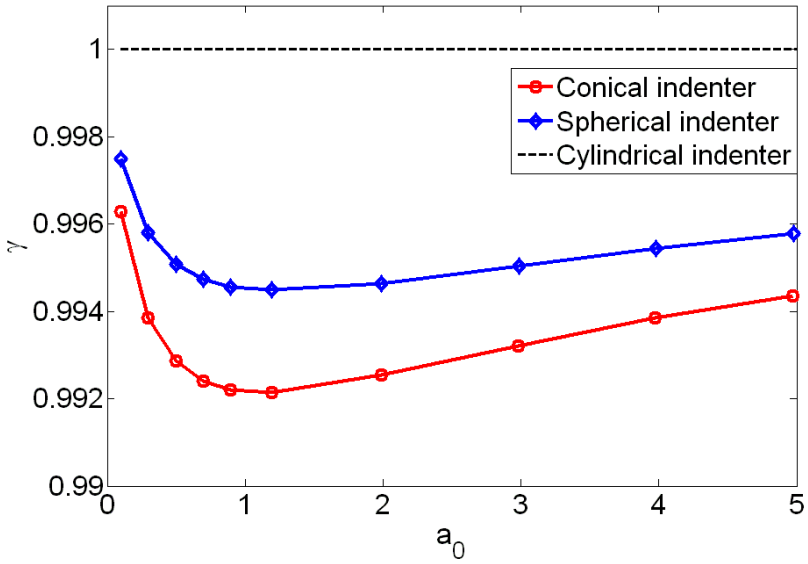

Fig. 4.2 Variation of parameter γ as function of radius of contact area a_0

The normal stress profile of the surface under the punch is of interest. Based on the analysis presented in Sect. 4.2, the contact stress under the punch at *z=0* is given by

$$\sigma_{zz} = -\frac{4\mu(\lambda+2\mu)d}{\pi a(\lambda+3\mu)}\left[\int_{r/a}^{1}\frac{H'(\tau)d\tau}{\sqrt{\tau^2-(r/a)^2}}-\frac{H(1)}{\sqrt{1-(r/a)^2}}\right] \qquad r/a<1 \qquad (4.45)$$

The corresponding classical solution was obtained by Sneddon [75] as:

(a) Flat ended punch

$$\sigma_{zz} = -\frac{4\mu(\lambda+\mu)d}{\pi a(\lambda+2\mu)}\frac{1}{\sqrt{1-(r/a)^2}} \qquad r/a<1 \qquad (4.46)$$

(b) Conical indenter

$$\sigma_{zz} = -\frac{4\mu(\lambda+\mu)d}{\pi a(\lambda+2\mu)}\log\left(\frac{1+\sqrt{1-(r/a)^2}}{r/a}\right) \qquad r/a<1 \qquad (4.47)$$

(c) Spherical indenter

$$\sigma_{zz} = -\frac{8\mu(\lambda+\mu)d}{\pi a(\lambda+2\mu)}\sqrt{1-(r/a)^2} \qquad r/a<1 \qquad (4.48)$$

Fig. 4.3-4.5 show the distribution of normal contact stresses under a punch with different profiles. The contact stress σ_{zz} is normalized as $\pi\sigma_{zz}/(4\mu d_0)$ and the radius r_0 as r_0/a_0. The broken line represents the classical solution. It is clear that the current solutions show the same trend as the classical solutions, and the surface energy effects have a negligible influence on the normal contact stresses, which is similar to the results of Chapter 2. When the radius of indenter is smaller, the effects of surface stresses are comparatively large.

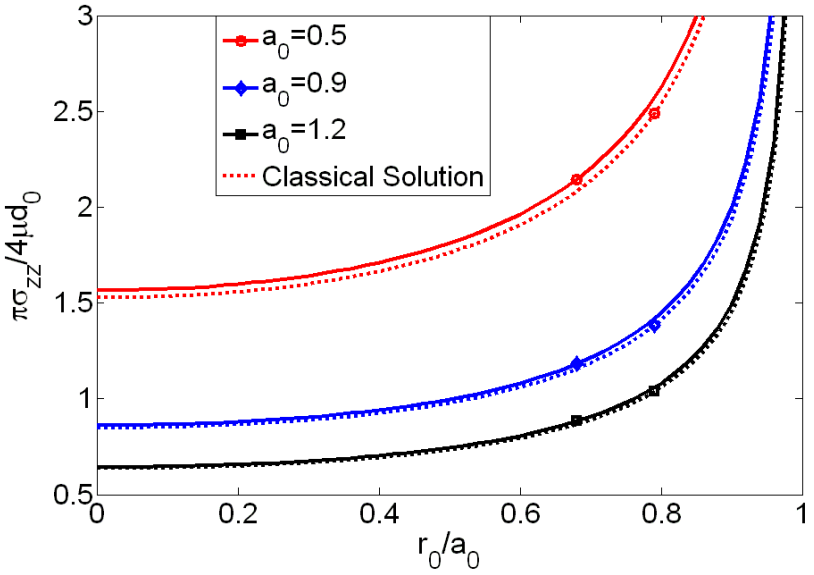

Fig. 4.3 Contact stress profiles under the punch for flat-ended cylindrical indenter

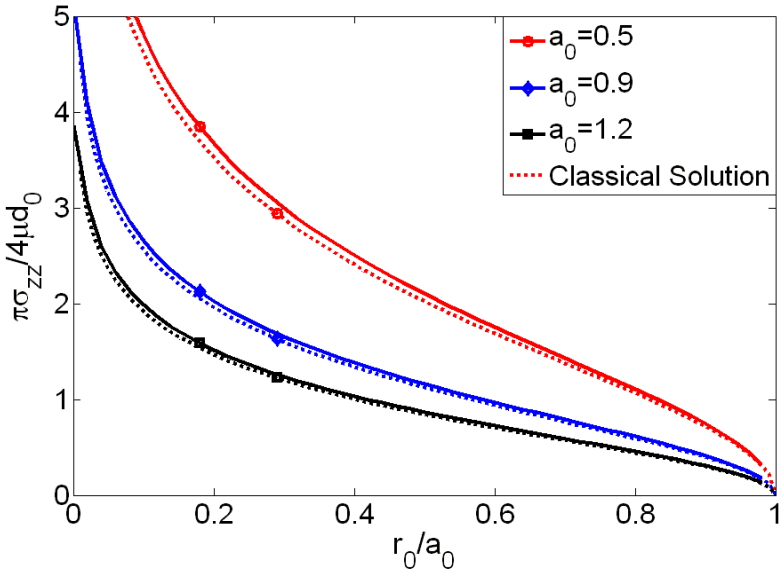

Fig. 4.4 Contact stress profiles under the punch for conical indenter

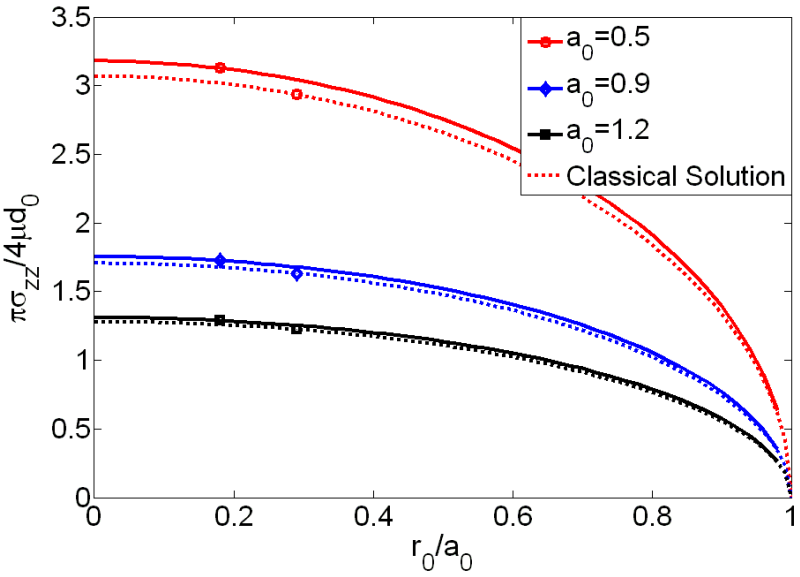

Fig. 4.5 Contact stress profiles under the punch for spherical indenter

Indentation force is a useful quantity in the indentation testing. Integrating the normal stresses of Eq. (4.46)-(4.48) over the contact area together with Eq. (4.36), the following load-indentation depth relationships can be obtained for the classical case and the non-classical case.

(a) For a flat-ended cylindrical indenter

$$P_c = \frac{8\mu(\lambda+\mu)}{\lambda+2\mu} a_c d$$
$$\frac{P}{P_c} = -\frac{(\lambda+2\mu)^2}{(\lambda+\mu)(\lambda+3\mu)} \int_0^1 H(\tau)\, d\tau \tag{4.49}$$

(b) For a conical indenter

$$P_c = \frac{4\mu(\lambda+\mu)}{\lambda+2\mu} a_c d$$
$$\frac{P}{P_c} = -\frac{2(\lambda+2\mu)^2}{(\lambda+\mu)(\lambda+3\mu)} \gamma \int_0^1 H(\tau)\, d\tau \tag{4.50}$$

(c) For a spherical tip indenter

$$P_c = \frac{16\mu(\lambda+\mu)}{3(\lambda+2\mu)} a_c d$$
$$\frac{P}{P_c} = -\frac{3(\lambda+2\mu)^2}{2(\lambda+\mu)(\lambda+3\mu)} \gamma \int_0^1 H(\tau)\, d\tau \tag{4.51}$$

where P_c is the indentation force in the classical case.

It can be seen from the above equations that the ratio P/P_c contains an integral part, in which the integrand function $H(\tau)$ is dependent on the radius of contact area a_0. It implies that P/P_c is dependent on the size of punch and the surface effect may play a role. Figure 4.6 shows the variation nondimensional total force ratio against the radius of contact area. It is seen that when the contact area becomes smaller, the total indentation force needed to make the same depth increases, which implies that the stiffness measured in the indentation experiment is dependent on the penetration depth for the conical and spherical indenter and depends on the radius of punch for the flat ended cylindrical indenter. The maximum influence surface effects is about 5% when $a_0 = 0.1$. However, for some soft gel materials whose intrinsic characteristic length is larger compared to the metals and the contact radius $a = a_0\Lambda$ is comparably higher, the influence of surface effects on the indentation force may be more prominent.

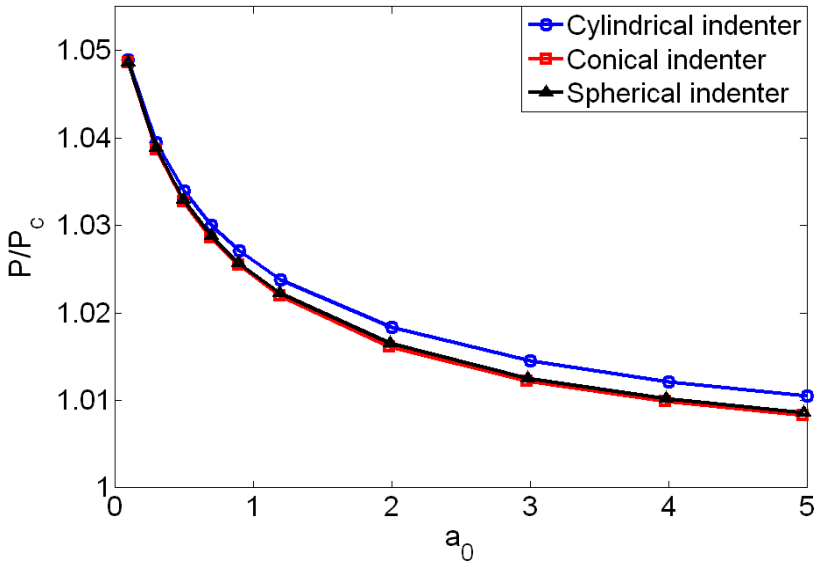

Fig. 4.6 Variation of nondimensional indentation force with the radius of contact area

Chapter 5

SUMMARY AND CONCLUSIONS

5.1 Summary and Major Findings

The main purpose of this thesis is to investigate the influence of surface energy effects on the stresses and deformations of nanoscale film/substrate systems and develop solutions based on the Gurtin-Murdoch elasticity model for surface loading and rigid indentation problems. The boundary-value problems considered in the present study are formulated by using Fourier and Hankel integral transform techniques. Selected numerical results are presented to portray the key features of the elastic field and the influence of surface energy effects. The conclusions of the current study are given below.

(1) Analytical solutions can be derived for the two-dimensional and axisymmetric elastic field of an isotropic compressible elastic layer of finite thickness that is bonded to a rigid base and subjected to surface loading. Closed-form solutions can be obtained for a half-plane subjected to a vertical or tangential point force and the solution can be separated into a classical part and a non-classical part that is governed by the surface elastic properties. In the case of a layer, numerical quadrature is required to compute the solutions expressed by semi-infinite integrals. A characteristic length, Λ, controlled by both surface material properties and bulk properties can be identified and the surface energy effects are solely controlled by Λ. Numerical results show that the influence of surface stresses is more significant under a horizontal load when compared to a vertical load. In the case of a vertical load, vertical displacement and normal stress show a small effect of surface energy but the horizontal displacement and horizontal stress have more visible influence. For Aluminum, the effect of surface energy becomes negligible at a distance greater than the material characteristic length for a vertical point load and twice the characteristic length for a horizontal point load. For a uniformly distributed axisymmetric load, the influence of surface energy effect is limited to a domain within two times the radius of loading area.

(2) The solution of a three-dimensional problem is demonstrated by considering the case of an isotropic elastic layer perfectly bonded to a rigid substrate and subjected to tangential surface loading. Hankel integral transforms are used to solve the boundary-value problems and analytical solutions are obtained for a tangential concentrated load and a uniformly distributed circular patch load. In the case of a semi-infinite medium, the solution for elastic field can be separated into a classical and a non-classical part to identify the influence of surface energy. As in the case of plane and axisymmetric loading problems, the characteristic length Λ governs the non-classical part of the solution. Selected numerical results show that the surface energy effects are confined to the region within 1.5 times the radius of loading area. The material generally becomes stiffer due to the surface energy effects leading to smaller displacements.

(3) The classical rigid indentation problem for an elastic layer is re-examined in this thesis in the presence of surface energy effects. The problem can be formulated in terms of a set of dual integral equations as in the classical case which can then be reduced to a Fredholm integral equation of the second kind. The solution to the integral equation is obtained using numerical quadrature. The numerical results show that the radius of contact area in the non-classical case is slightly lower than the classical solution for conical and spherical indenters and depends on the size of indenter for all three types of indenters. A similar size-dependent behavior is also observed for the total indentation force and the results show that the surface energy effect causes material to behave stiffer. In general the influence of surface energy effects on vertical indentation is quite small but can be substantial for lateral loading cases.

5.2 Suggestions for Future Work

The present thesis has examined only the basic loading and contact problems for a thin elastic layer. It is recommended that following studies be undertaken to further improve understanding of the nanomechanics of film/substrate systems and the mechanics of soft solids.

(1) In most practical cases the substrate is not rigid. It is very useful to examine the influence of an elastic substrate in the presence of both surface and interface energy effects. The current methodology based on Fourier and Hankel transforms can be readily extended to solve the case of a flexible substrate.

(2) Isotropic behavior of film/substrate is another limitation of the present study. It is useful to consider an anisotropic film/substrate system. Stroh's formalism that is widely used in classical anisotropic elasticity can be extended to formulate the case of an anisotropic film/substrate system.

(3) The indentation problem was solved only for a semi-infinite medium. It would be useful to consider the indentation of a film/substrate system to simulate a practical case. In addition, the solution for lateral loading is also useful in simulating multidimensional indentation techniques [80] used for material characterization

(4) Experimental studies are needed to measure the surface elastic constants and validate the applicability of Gurtin-Murdoch model. Current results show that the surface energy effect has a more significant influence on the elastic field under a tangential load compared to a vertical load. Therefore, it is suggested that multidimensional contact mechanic experiments be used to measure the surface elastic constants and compared with properties determined using atomistic simulations.

Bibliography

[1] Calvert, P., 1996, "Rough Guide to the Nanoworld," Nature, **383**(6598) pp. 300-301.

[2] Feynman, R., 1960, "There's Plenty of Room at the Bottom: An Invitation to Enter a New Field of Physics," Engineering and Science, **23**(5) pp. 22–36.

[3] Drexler, K.E., and Whitaker, R., 1986, "Engines of creation: the coming era of nanotechnology," Anchor Books, New York.

[4] Mackerle, J., 2005, "Nanomaterials, Nanomechanics and Finite Elements: A Bibliography(1994–2004)," Modelling and Simulation in Materials Science and Engineering, **13**(1) pp. 123-158.

[5] Iijima, S., 1991, "Helical Microtubules of Graphitic Carbon," Nature, **354**(6348) pp. 56-58.

[6] Iijima, S., and Ichihashi, T., 1993, "Single-Shell Carbon Nanotubes of 1-Nm Diameter," Nature, **363**(6430) pp. 603-605.

[7] Peng, B., Locascio, M., Zapol, P., Li, S., Mielke, S.L., Schatz, G.C. and Espinosa, H.D., 2008, "Measurements of Near-Ultimate Strength for Multiwalled Carbon Nanotubes and Irradiation-Induced Crosslinking Improvements," Nature Nanotechnology, **3**(10) pp. 626-631.

[8] Vendamme, R., Onoue, S. Y., Nakao, A., and Kunitake, T., 2006, "Robust Free-Standing Nanomembranes of organic/inorganic Interpenetrating Networks," Nature Materials, **5**(6) pp. 494-501.

[9] Deneen, J., Mook, W. M., Minor, A., Gerberich, W. W., and Barry, C. C., 2006, "In Situ Deformation of Silicon Nanospheres," Journal of Materials Science, **41**(14) pp. 4477-4483.

[10] Zhang, G. P., Sun, K. H., Zhang, B., Gong, J., Sun, C., and Wang, Z. G., 2008, "Tensile and Fatigue Strength of Ultrathin Copper Films," Materials Science and Engineering: A, **483-484** pp. 387-390.

[11] Zhu, Y., Yukimura, K., Ding, C., and Zhang, P., 2001, "Tribological Properties of Nanostructured and Conventional WC–Co Coatings Deposited by Plasma Spraying," Thin Solid Films, **388**(1-2) pp. 277-282.

[12] Wilson, M., Kannangara, K., Smith, G., Simmons, M., and Raguse, B., 2002, "Nanotechnology: Basic science and emerging technologies," Chapman & Hall/CRC, New York.

[13] Hochella, J. M. F., 2002, "There's Plenty of Room at the Bottom: Nanoscience in Geochemistry," Geochimica Et Cosmochimica Acta, **66**(5) pp. 735-743.

[14] Liu, W. K., Park, H. S., Qian, D., Karpov, E. G., Kadowaki, H., and Wagner, G.J., 2006, "Bridging Scale Methods for Nanomechanics and Materials," Computer Methods in Applied Mechanics and Engineering, **195**(13-16) pp. 1407-1421.

[15] Qian, D., Liu, W. K., and Zheng, Q., 2008, "Concurrent quantum/continuum Coupling Analysis of Nanostructures," Computer Methods in Applied Mechanics and Engineering, **197**(41-42) pp. 3291-3323.

[16] Liu, W. K., Karpov, E. G., Zhang, S., and Park, H. S., 2004, "An Introduction to Computational Nanomechanics and Materials," Computer Methods in Applied Mechanics and Engineering, **193**(17-20) pp. 1529-1578.

[17] Kouris, D., and Gao, H., 2002, "Nanomechanics of Surfaces and Interfaces," Journal of Applied Mechanics - Transactions of the ASME, **69**(4) pp. 405-406.

[18] Li, S., and Wang, G., 2008, "Introduction to micromechanics and nanomechanics," World Scientific Pub., Singapore.

[19] Dingreville, R., Qu, J. M., and Cherkaoui, M., 2005, "Surface Free Energy and its Effect on the Elastic Behavior of Nano-Sized Particles, Wires and Films," Journal of the Mechanics and Physics of Solids, **53**(8) pp. 1827-1854.

[20] Dingreville, R., and Qu, J. M., 2008, "Interfacial Excess Energy, Excess Stress and Excess Strain in Elastic Solids: Planar Interfaces," Journal of the Mechanics and Physics of Solids, **56**(5) pp. 1944-1954.

[21] Wong, E. W., Sheehan, P. E., and Lieber, C. M., 1997, "Nanobeam Mechanics: Elasticity, Strength, and Toughness of Nanorods and Nanotubes," Science, **277**(5334) pp. 1971.

[22] Yu, M. F., Lourie, O., Dyer, M. J., Moloni, K., Kelly, T. F., and Ruoff, R. S., 2000, "Strength and Breaking Mechanism of Multiwalled Carbon Nanotubes Under Tensile Load," Science, **287**(5453) pp. 637.

[23] Beegan, D., Chowdhury, S., and Laugier, M. T., 2007, "Comparison between Nanoindentation and Scratch Test Hardness (Scratch Hardness) Values of Copper Thin Films on Oxidised Silicon Substrates," Surface and Coatings Technology, **201**(12) pp. 5804-5808.

[24] Oliver, W. C., and Pharr, G. M., 2004, "Measurement of Hardness and Elastic Modulus by Instrumented Indentation: Advances in Understanding and Refinements to Methodology," Journal of Materials Research, **19**(1) pp. 3-20.

[25] Pharr, G. M., Oliver, W. C., and Brotzen, F. R., 1992, "On the Generality of the Relationship among Contact Stiffness, Contact Area, and Elastic Modulus during Indentation," Journal of Materials Research, **7**(3) pp. 613-617.

[26] Bull, S. J., 2005, "Nanoindentation of Coatings," Journal of Physics D-Applied Physics, **38**(24) pp. 393-413.

[27] Oliver, W. C., and Pharr, G. M., 1992, "Improved Technique for Determining Hardness and Elastic Modulus using Load and Displacement Sensing Indentation Experiments," Journal of Materials Research, **7**(6) pp. 1564-1583.

[28] Mao, S. X., Zhao, M., and Wang, Z. L., 2003, "Nanoscale Mechanical Behavior of Individual Semiconducting Nanobelts," Applied Physics Letters, **83** pp. 993.

[29] Li, X., Gao, H., Murphy, C. J., and Caswell, K. K., 2003, "Nanoindentation of Silver Nanowires," Nano Letters, **3**(11) pp. 1495-1498.

[30] Gibbs, J.W., 1906, "The scientific papers of J. Willard Gibbs," Dover Publications, Inc, New York.

[31] Shuttleworth, R., 1950, "The Surface Tension of Solids," Proceedings of the Physical Society Section A, **63**(5) pp. 444-457.

[32] Cammarata, R. C., 1994, "Surface and Interface Stress Effects in Thin Films," Progress in Surface Science, **46**(1) pp. 1-38.

[33] Fried, E., and Gurtin, M. E., 2004, "A Unified Treatment of Evolving Interfaces Accounting for Small Deformations and Atomic Transport with Emphasis on Grain-Boundaries and Epitaxy," Advances in Applied Mechanics, **40** pp. 1-177.

[34] Fischer, F. D., Waitz, T., Vollath, D., and Simha, N. K., 2008, "On the Role of Surface Energy and Surface Stress in Phase-Transforming Nanoparticles," Progress in Materials Science, **53**(3) pp. 481-527.

[35] Cahn, J. W., 1979, "Thermodynamics of solid and fluid surfaces," Interfacial Segregation, Anonymous American Society for Metals, pp. 3-23.

[36] Cammarata, R. C., 1997, "Surface and Interface Stress Effects on Interfacial and Nanostructured Materials," Materials Science and Engineering A, **237**(2) pp. 180-184.

[37] Nix, W. D., and Gao, H., 1998, "An Atomistic Interpretation of Interface Stress," Scripta Materialia, **39**(12) pp. 1653-1661.

[38] Sander, D., 2003, "Surface Stress: Implications and Measurements," Current Opinion in Solid State and Materials Science, **7**(1) pp. 51-57.

[39] Miller, R. E., and Shenoy, V. B., 2000, "Size-Dependent Elastic Properties of Nanosized Structural Elements," Nanotechnology, **11**(3) pp. 139-147.

[40] Gurtin, M. E., and Murdoch, A. I., 1975, "A Continuum Theory of Elastic Material Surfaces," Archive for Rational Mechanics and Analysis, **57**(4) pp. 291-323.

[41] Gurtin, M. E., and Murdoch, A. I., 1978, "Surface Stress in Solids," International Journal of Solids and Structures, **14**(6) pp. 431–440.

[42] Gurtin, M. E., Weissmuller, J., and Larche, F., 1998, "A General Theory of Curved Deformable Interfaces in Solids at Equilibrium," Philosophical Magazine A, **78**(5) pp. 1093-1109.

[43] Dingreville, R., and Qu, J., 2007, "A Semi-Analytical Method to Compute Surface Elastic Properties," Acta Materialia, **55**(1) pp. 141-147.

[44] Dingreville, R., Kulkarni, A. J., Zhou, M., and Qu, J., 2008, "A Semi-Analytical Method for Quantifying the Size-Dependent Elasticity of Nanostructures," Modelling and Simulation in Materials Science and Engineering, **16**(2) pp. 25002-25002.

[45] Shenoy, V. B., 2005, "Atomistic Calculations of Elastic Properties of Metallic Fcc Crystal Surfaces," Physical Review B, **71**(9) pp. 094104.

[46] Mi, C., Jun, S., Kouris, D. A., and Kim, S. Y., 2008, "Atomistic Calculations of Interface Elastic Properties in Noncoherent Metallic Bilayers," Physical Review B, **77**(7) pp. 075425.

[47] Jing, G. Y., Duan, H. L., Sun, X. M., Zhang, Z.S., Xu, J., Li, Y.D., Wang, J.X., and Yu, D.P., 2006, "Surface Effects on Elastic Properties of Silver Nanowires: Contact Atomic-Force Microscopy," Physical Review B, **73**(23) pp. 235409.

[48] He, J., and Lilley, C. M., 2008, "Surface Effect on the Elastic Behavior of Static Bending Nanowires," Nano Letters, **8**(7) pp. 1798-1802.

[49] He, J., and Lilley, C. M., 2008, "Surface Stress Effect on Bending Resonance of Nanowires with Different Boundary Conditions," Applied Physics Letters, **93**pp. 263108.

[50] Wang, G. F., and Feng, X. Q., 2007, "Effects of Surface Elasticity and Residual Surface Tension on the Natural Frequency of Microbeams," Applied Physics Letters, **90**pp. 231904.

[51] Gurtin, M. E., Markenscoff, X., and Thurston, R. N., 1976, "Effect of Surface Stress on the Natural Frequency of Thin Crystals," Applied Physics Letters, **29**pp. 529.

[52] Lu, P., Lee, H. P., Lu, C., 2005, "Surface Stress Effects on the Resonance Properties of Cantilever Sensors," Physical Review B, **72** pp. 085405.

[53] Lachut, M. J., and Sader, J. E., 2007, "Effect of Surface Stress on the Stiffness of Cantilever Plates," Physical Review Letters, **99** pp. 206102.

[54] Park, H. S., 2009, "Quantifying the Size-Dependent Effect of the Residual Surface Stress on the Resonant Frequencies of Silicon Nanowires if Finite Deformation Kinematics are Considered," Nanotechnology, **20**(115701) pp. 115701.

[55] He, L. H., Lim, C. W., and Wu, B. S., 2004, "A Continuum Model for Size-Dependent Deformation of Elastic Films of Nano-Scale Thickness," International Journal of Solids and Structures, **41**(3-4) pp. 847-857.

[56] Huang, D. W., 2008, "Size-Dependent Response of Ultra-Thin Films with Surface Effects," International Journal of Solids and Structures, **45**(2) pp. 568-579.

[57] Lu, P., He, L. H., Lee, H. P., and Lu, C., 2006, "Thin Plate Theory Including Surface Effects," International Journal of Solids and Structures, **43**(16) pp. 4631-4647.

[58] Sharma, P., Ganti, S., and Bhate, N., 2003, "Effect of Surfaces on the Size-Dependent Elastic State of Nano-Inhomogeneities," Applied Physics Letters, **82**pp. 535.

[59] Sharma, P., and Wheeler, L. T., 2007, "Size-Dependent Elastic State of Ellipsoidal Nano-Inclusions Incorporating Surface⁄ Interface Tension," Journal of Applied Mechanics - Transactions of the ASME, **74**(3) pp. 447-454.

[60] Tian, L., and Rajapakse, R. K. N. D., 2007, "Analytical Solution for Size-Dependent Elastic Field of a Nanoscale Circular Inhomogeneity," Journal of Applied Mechanics - Transactions of the ASME, **74**(3) pp. 568-574.

[61] Tian, L., and Rajapakse, R. K. N. D., 2007, "Elastic Field of an Isotropic Matrix with a Nanoscale Elliptical Inhomogeneity," International Journal of Solids and Structures, **44**(24) pp. 7988-8005.

[62] Duan, H. L., Wang, J., Huang, Z. P., and Karihaloo, B. L., 2005, "Size-Dependent Effective Elastic Constants of Solids Containing Nano-Inhomogeneities with Interface Stress," Journal of the Mechanics and Physics of Solids, **53**(7) pp. 1574-1596.

[63] Duan, H. L., Wang, J., Huang, Z. P., and Luo, Z. Y., 2005, "Stress Concentration Tensors of Inhomogeneities with Interface Effects," Mechanics of Materials, **37**(7) pp. 723-736.

[64] Duan, H. L., Wang, J., Huang, Z. P., and Karihaloo, B. L., 2005, "Eshelby Formalism for Nano-Inhomogeneities," Proceedings of the Royal Society A, **461**(2062) pp. 3335-3353.

[65] Duan, H. L., WANG, J., and Karihaloo, B. L., 2008, "Theory of Elasticity at the Nanoscale," Advances in Applied Mechanics, **42** pp. 1-68.

[66] Gao, W., Yu, S. W., and Huang, G. Y., 2006, "Finite Element Characterization of the Size-Dependent Mechanical Behaviour in Nanosystems," Nanotechnology, **17**(4) pp. 1118-1122.

[67] Tian, L., and Rajapakse, R. K. N. D., 2007, "Finite Element Modelling of Nanoscale Inhomogeneities in an Elastic Matrix," Computational Materials Science, **41**(1) pp. 44-53.

[68] Nix, W. D., 2005, "Mechanical Properties of Thin Films," Lecture Note, Stanford University.

[69] Vinci, R. P., and Vlassak, J. J., 1996, "Mechanical Behavior of Thin Films," Annual Review of Materials Science, **26**(1) pp. 431-462.

[70] Mishnaevsky Jr, L. L., and Gross, D., 2005, "Deformation and Failure in Thin films/substrate Systems: Methods of Theoretical Analysis," Applied Mechanics Reviews, **58**pp. 338.

[71] Feng, X., Huang, Y., and Rosakis, A. J., 2008, "Stresses in a Multilayer Thin Film/Substrate System Subjected to Nonuniform Temperature," Journal of Applied Mechanics - Transactions of the ASME, **75** pp. 021022.

[72] Ngo, D., Feng, X., Huang, Y., and Rosakis, A. J., 2008, "Multilayer Thin films/substrate System with Variable Film Thickness Subjected to Non-Uniform Misfit Strains," Acta Materialia, **56**(18) pp. 5322-5328.

[73] Poulos, H. G., 1967, "Stresses and Displacements in an Elastic Layer Underlain by a Rough Rigid Base," Geotechnique, **17**(4) pp. 378-410.

[74] Harding, J. W., and Sneddon, I. N., 1945, "The Elastic Stresses Produced by the Indentation of the Plane Surface of a Semi-Infinite Elastic Solid by a Rigid Punch," Proceedings of the Cambridge Philosophical Society, **41**(01) pp. 16-26.

[75] Sneddon, I. N., 1965, "The Relation between Load and Penetration in the Axisymmetric Boussinesq Problem for a Punch of Arbitrary Profile," International Journal of Engineering Science, **3**(1) pp. 47-57.

[76] Lebedev, N. N., and Ufliand, I. S., 1958, "Axisymmetric Contact Problem for an Elastic Layer," Journal of Applied Mathematics and Mechanics, **22**(3) pp. 442-450.

[77] Dhaliwal, R. S., and Rau, I. S., 1970, "The Axisymmetric Boussinesq Problem for a Thick Elastic Layer Under a Punch of Arbitrary Profile," International Journal of Engineering Science, **8**(10) pp. 843-856.

[78] Rau, I. S., and Dhaliwal, R. S., 1972, "Further Considerations on the Axisymmetric Boussinesq Problem," International Journal of Engineering Science, **10**(8) pp. 659-663.

[79] Yu, H. Y., Sanday, S. C., and Rath, B. B., 1990, "The Effect of Substrate on the Elastic Properties of Films Determined by the Indentation Test — Axisymmetric Boussinesq Problem," Journal of the Mechanics and Physics of Solids, **38**(6) pp. 745-764.

[80] Lucas, B. N., Hay, J. C., and Oliver, W. C., 2004, "Using Multidimensional Contact Mechanics Experiments to Measure Poisson's Ratio," Journal of Materials Research, **19**(1) pp. 58-65.

[81] Gao, Y. F., Xu, H. T., Oliver, W. C., and Pharr, G. M., 2008, "Effective Elastic Modulus of Film-on-Substrate Systems Under Normal and Tangential Contact," Journal of the Mechanics and Physics of Solids, **56**(2) pp. 402-416.

[82] Povstenko, Y. Z., 1993, "Theoretical Investigation of Phenomena Caused by Heterogeneous Surface Tension in Solids," Journal of the Mechanics and Physics of Solids, **41**(9) pp. 1499-1514.

[83] He, L. H., and Lim, C. W., 2006, "Surface Green Function for a Soft Elastic Half-Space: Influence of Surface Stress," International Journal of Solids and Structures, **43**(1) pp. 132-143.

[84] Wang, G. F., and Feng, X. Q., 2007, "Effects of Surface Stresses on Contact Problems at Nanoscale," Journal of Applied Physics, **101** pp. 013510.

[85] Huang, G. Y., and Yu, S. W., 2007, "Effect of Surface Elasticity on the Interaction between Steps," Journal of Applied Mechanics, **74** pp. 821.

[86] Koguchi, H., 2008, "Surface Green Function with Surface Stresses and Surface Elasticity using Stroh's Formalism," Journal of Applied Mechanics - Transactions of the ASME, **75**pp. 061014.

[87] Muki, R., 1960, "Asymmetric Problems of the Theory of Elasticity for a Semi-Infinite Solid and a Thick Plate," Progress in Solid Mechanics, **1** pp. 400-439.

[88] Sneddon, I.N., 1951, "Fourier transforms," McGraw-Hill., New York.

[89] Selvadurai, A.P.S., 2000, "Partial Differential Equations in Mechanics," Springer, Berlin; New York.

[90] Pickett, G., 1938, "Stress distribution in a loaded soil with some rigid boundaries," Proc. Highway Res. Board, Anonymous Highway Research Board, **18,** pp. 35-48.

[91] Meyers, M.A., and Chawla, K.K., 1999, "Mechanical behavior of materials," Prentice Hall, Upper Saddle River, New Jersey, USA.

[92] Noble, B., 1963, "The Solution of Bessel Function Dual Integral Equations by a Multiplying-Factor Method," Mathematical Proceedings of the Cambridge Philosophical Society, **59,** pp. 351-362.

[93] Ouyang, G., Yang, G., Sun, C., and Zhu, W., 2008, "Nanoporous structures: smaller is stronger," Small, **4**, pp. 1359-1362.